Fracture closure in extension and mechanical interaction of parallel joints

Leonid N. Germanovich
School of Civil and Environmental Engineering, Georgia Institute of Technology, Atlanta, Georgia, USA

Dmitriy K. Astakhov
Pinnacle Technologies, Inc., Bakersfield, California, USA

Received 1 August 2002; accepted 2 January 2003; published 24 February 2004.

[1] It is well known that in many cases rock permeability depends upon in situ stress conditions and on the pressure of the flowing fluid. Parallel and quasi-parallel joints represent one of the most often observed permeability structures. Frequently, joint sets are closely spaced and although joint mechanical interaction could significantly affect their aperture, the interaction is usually ignored in the evaluation of permeability. In this paper, on the basis of accurate computations of the interaction between the parallel fractures and conducted physical experiments, we suggest that the internal pressure can, in fact, close the pressurized joints. In general, there is a critical spacing between the parallel fractures below which their surfaces start contacting under the extensional load. However, the two edge fractures (end members) in the set remain widely open because they are not suppressed from one side. These effects dramatically change rock permeability and the fluid flow pattern. *INDEX TERMS:* 5104 Physical Properties of Rocks: Fracture and flow; 5114 Physical Properties of Rocks: Permeability and porosity; 5139 Physical Properties of Rocks: Transport properties; 8010 Structural Geology: Fractures and faults; 8020 Structural Geology: Mechanics; *KEYWORDS:* permeability, joints, parallel fractures, crack interaction, fluid flow

Citation: Germanovich, L. N., and D. K. Astakhov (2004), Fracture closure in extension and mechanical interaction of parallel joints, *J. Geophys. Res.*, *109*, B02208, doi:10.1029/2002JB002131.

1. Introduction

[2] Joints (open mode brittle fractures) are probably the most common brittle structures in the Earth's crust [*Pollard and Aydin*, 1988]. In layered sedimentary rocks, joints are commonly perpendicular to the bedding planes and are often confined within one layer [e.g., *McQuillan*, 1973; *Ladeira and Price*, 1981; *Narr and Suppe*, 1991]. The extensive interest in joint formation, propagation, and interaction is explained by the key role that joints play in water and hydrocarbon transport through the crust [*Long et al.*, 1996]. Also, joints are commonly used to estimate the strain accumulated in rock formations (e.g., by the scan line method [see *Hudson and Priest*, 1979; *Bai et al.*, 2000]). It is now widely accepted that two main mechanisms are responsible for jointing. One is cracking due to the far-field extension [e.g., *Hobbs*, 1967; *Pollard and Segall*, 1987; *Ji and Saruwatari*, 1998]. The other one is hydraulic fracturing caused by the pressurized fluid [e.g., *Secor*, 1965; *Engelder and Lacazette*, 1990; *Fischer et al.*, 1995; *Cosgrove*, 1997]. In this work, we do not consider joint formation, concentrating instead on the opening of already existing joints (Figure 1). Accordingly, we focus on the effects of joints on rock permeability rather than on studying the joint spacing [e.g., see *Ji and Saruwatari*, 1998] or relation to other geological features [e.g., *Zhao and Johnson*, 1992].

[3] In fact, numerous field and laboratory studies have provided significant information about joint spacing in various geological settings (e.g., see the review by *Pollard and Aydin* [1988]). Joints are often confined in mechanical layers [e.g., *Gross*, 1993; *Bai et al.*, 2000] and, therefore, have approximately the same size, $2c$, as the layer thickness [e.g., *Becker and Gross*, 1996]. In this work, to characterize the joint density, we use the normalized joint spacing, $s = b/(2c)$, where b is the dimensional spacing between the joints (Figure 2a). Clearly, the lower values of s correspond to denser joint sets. The obvious upper theoretical limit of fracture spacing ratio is $s \rightarrow \infty$, which corresponds to isolated (noninteracting) joints and an infinite value of normalized joint spacing. Further in the text, for the sake of briefness, normalized joint spacing is called simply spacing.

[4] Although in some publications spacing reported from the field observations varies only from 0.7 to 1.7 [*Narr and Suppe*, 1991; *Becker and Gross*, 1996], there is ample evidence of much smaller spacing. For example, the data reported by *Ladeira and Price* [1981] for the shale beds in Flysch (UK) corresponds to the spacing ranging from 0.02 to 1.25. *McQuillan* [1973] provides the results of measurements of the fracture density in Asmari formation (Iran)

0148-0227/04/2002JB002131$09.00

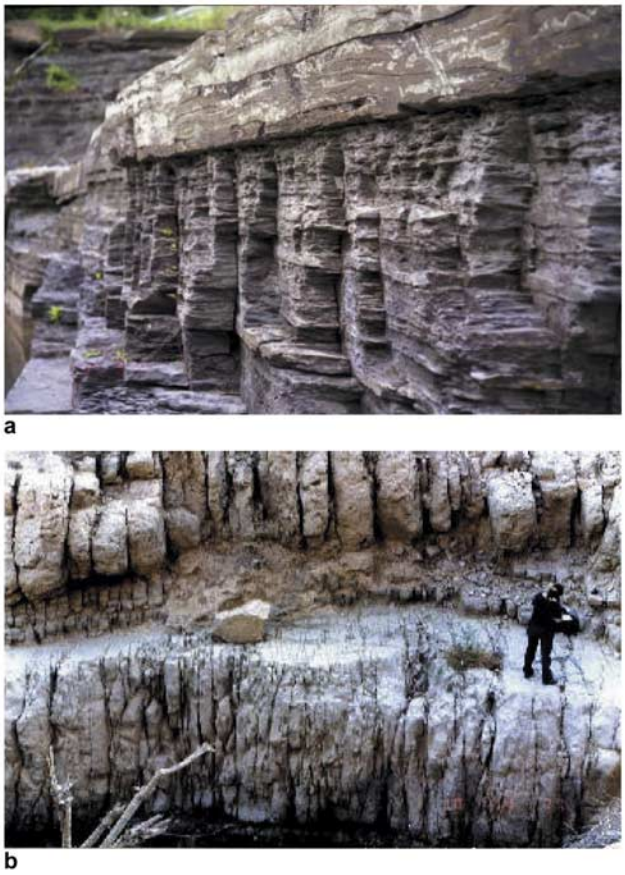

Figure 1. (a) A set of parallel joints in the alternating siltstone and shale beds on the Appalachian Plateau near Finger Lakes, central New York (courtesy of B. Carter; see also *Helgeson and Aydin* [1991] and *Engelder et al.* [1999]). (b) Subparallel joints in a dolomite layer near the central Dead Sea area [see *Sagy et al.*, 2001].

suggesting spacing varying from 0.1 to 3 (see also Figure 1). *Reches* [1998] reported joint spacing in limestone layers within the Carmel Formation, Utah, ranging from 0.03 through 0.1. *Sagy et al.* [2001] observed joint spacing in dolomite layers in the Dead Sea Rift margins (Israel) varying from 0.05 to 0.5.

[5] The information on the density of fractures and their sizes can be used to estimate rock permeability [e.g., *Nehlig and Juteau*, 1988; *van Everdingen*, 1995; *Germanovich et al.*, 2000]. Fracture density and apertures are often mapped [e.g., *Hudson and Priest*, 1979] and then the permeability can be calculated on the basis of one or another fracture network model [e.g., *Dershowitz and Einstein*, 1988; *Berkowitz*, 1994]. For example, *van Everdingen* [1995] employed parallel plate, matrix addition, and stochastic methods. All these methods assume that the openings of all joints in the set are the same when the fluid flows through them and when the fracture aperture measurements are performed. In this work, we show that this may not always be the case and, as a result, the permeability pattern may be highly heterogeneous, even at the macroscale.

[6] Most models of stress-dependent permeability of fractured rocks are based on the concept of single, noninteracting fractures [e.g., *Gangi*, 1978; *Tsang and Witherspoon*, 1981; *Gavrilenko and Gueguen*, 1989; *David*, 1993]. It has been recognized only recently [*Nolte*, 1987; *Germanovich et al.*, 1998b; *Bai and Pollard*, 2001] that elastic interaction between the joints can also become an important factor affecting rock permeability and fluid flow distribution.

[7] In general, to evaluate the elastic interaction, one has to consider the corresponding problem for multiple interacting cracks. The stress field near an isolated pressurized crack in the homogeneous or layered, elastic medium has been thoroughly studied both in general [e.g., *Sneddon*, 1951] and as applied to geological situations [e.g., *Pollard and Segall*, 1987; *Fischer et al.*, 1995]. The interaction between the cracks becomes significant if these are spaced sufficiently close to each other so that the crack spacing is comparable to or smaller than their sizes. To the best of our knowledge, rigorous closed form solutions of such problems are not available even for two cracks, unless they are located along a straight line [*Muskhelishvili*, 1953]. An alternative could be, in principle, an estimate based on one or another physical assumption [*Nolte*, 1987; *Palmer and Veatch*, 1990]. The remaining feasible alternatives are numerical [e.g., *Theocaris and Chrysakis*, 1983; *Jeffrey et al.*, 1987; *Bai et al.*, 2000] and asymptotic [e.g., *Koiter*, 1961; *Isida*, 1973; *Datsyshin and Savruk*, 1974] approaches, which are implemented in this work.

[8] In this paper, we examine the effect of elastic interaction on the apertures of joints in various joint sets. We consider spacing, s, that varies in the range of 10^{-2}–10, which likely covers all of the observed values of spacing reported in the literature (see above). We show that not only it is necessary to take into account the interaction between the joints if $s < 1$, but also that for $s < 0.1$, which is not unusual (e.g., see Figures 1a and 1b), joints can be closed by the internal fluid pressure. The obtained results are further applied to study stress-dependent permeability of jointed rock [*Germanovich and Astakhov*, 2004].

2. Elastic Problem for Interacting Joints

[9] As mentioned in section 1, joints are often confined within one mechanical layer which, in fact, can include one or more lithological layers [e.g., *Bai et al.*, 2000]. *Fischer et al.* [1995] showed that the relative thickness of jointed and adjacent layers practically does not affect the stress component normal to the joints in the jointed layer. If the joint length in the z direction is considerably greater than in the x direction (Figure 2a), it is permissible to consider joint interaction in each cross section, z = const, in a two-dimensional approximation of plane strain and independently of other cross sections.

[10] This approximation is widely accepted for such processes associated with laterally elongated fractures as joint formation [e.g., *Bai et al.*, 2000] and hydraulic fracturing [e.g., see *Germanovich et al.*, 1997a, 1998b, and references cited therein]. In the case under consideration, the approximation is sufficiently accurate if the pressure gradient, dp/dz, is not too high, that is, the typical spatial scale, L_p, of changing pressure in the z direction (Figure 2a) is appreciably greater than the joint size, $2c$. Then, the simple scaling, $p/L_p \ll p/(2c)$, results in the

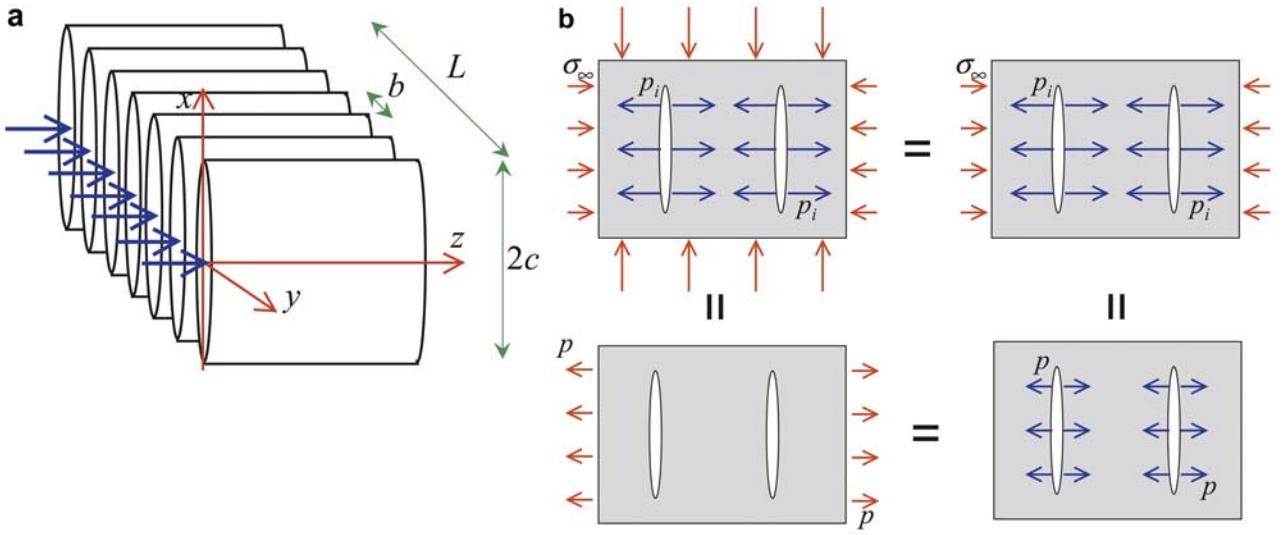

Figure 2. (a) A set of parallel, equally sized and spaced joints and (b) joints opened by extensional loads ($p = p_i - \sigma_\infty$) that are equivalent with respect to joint openings and stress intensity factors. In particular, the internal pressure, p, is equivalent to the remote loading of the same magnitude.

condition of $dp/dz \ll p/(2c)$ that is further assumed to be satisfied. For higher pressure gradients, plane solution may not qualify anymore and three dimensionality may have to be introduced explicitly. Similarly, although conjugate or even perpendicular sets of joints are rather frequently observed in situ, in this work we consider only sets of parallel joints and ignore the 3-D effects of other families of joints on our solution.

[11] Therefore, for the most typical case of joints perpendicular to the bedding planes and stresses acting parallel to the beds, an infinite elastic plane with the corresponding set of parallel interacting cracks can be considered with sufficient accuracy. Since in linear crack theory, the remote load acting along parallel, rectilinear fractures does not affect their openings [e.g., *Parker*, 1981], it will be ignored in the following consideration (Figure 2b). Furthermore, if the far-field conditions are specified in terms of strains rather than stresses, the application of Hook's law (as in the work by *Bai et al.* [2000]) to the homogeneous remote stress-strain field obviously allows simple respecification of the remote conditions in terms of stresses. Finally, within linear elastic theory, the superposition principle [e.g., *Parker*, 1981] suggests that the openings of pressurized cracks do not change if the equal load is instead applied at infinity (Figure 2b). Therefore, in the forthcoming analysis, we do not distinguish between these two cases but simply refer to them as extensional loading. In other words, we call the load extensional, if it would open a single (isolated) fracture resulting in fracture dilation. In this sense, either pressurizing the fracture internally or applying remote tension (Figure 2b) dilates (opens) it equally. It is understood that the stress fields are not the same for these two cases (e.g., compression versus tension) and differ by the uniaxial tension p (Figure 2b). Yet, the crack opening displacements and stress intensity factors are mathematically identical in both cases.

[12] The boundary conditions on the joint sides can be written as

$$\sigma_{yy} = -p, \quad \tau_{xy} = 0 \quad (-c < x < c,\ y = 0,\ p \geq 0) \qquad (1)$$

where σ_{ij} ($i, j = x, y$) are the stresses in the elastic plane (cross section) under consideration. Note that it is mathematically consistent to specify both the pressure, p, and pressure gradient, $\partial p/\partial z$ (see the previous section), in the same cross section since these quantities are then uniquely defined in all other cross sections. From the physical standpoint, however, this assumption is not essential but makes the comparison of the studied, k, and reference, k_0, permeabilities technically simpler [*Germanovich and Astakhov*, 2004].

[13] In crack theory, the problem of elastic interaction has been addressed in many publications [e.g., *Smith*, 1966; *Delameter et al.*, 1975; *Panasyuk et al.*, 1977; *Chudnovsky et al.*, 1987; *McCartney and Gorley*, 1987; *Kachanov*, 1987, 1993; *Hu et al.*, 1993; *Dyskin and Mühlhaus*, 1995; *Chen*, 1995; *Galybin*, 1998], including those devoted to various geological settings [e.g., *Lachenbruch*, 1961; *Delaney and Pollard*, 1981; *Delaney et al.*, 1986; *Du and Aydin*, 1991; *Olson and Pollard*, 1991; *Olson*, 1993; *Reches and Lockner*, 1994; *Willemse et al.*, 1996; *Germanovich et al.*, 1997b, 1998a; *Renshaw and Park*, 1997; *Martel and Boger*, 1998]. Here we use the boundary collocation method (BCM) [e.g., *Isida*, 1971; *Parker*, 1981; *Aliabadi and Rooke*, 1991; *Lam and Phua*, 1991] to compute the opening of interacting joints. The version of BCM implemented in this work is similar to that of *Gladwell and England* [1977] and *McCartney and Gorley* [1987], who expanded the modified *Muskheleshvili*'s [1953] complex potentials into series with respect to the Chebyshev polynomials and then used the boundary conditions assigned on the crack sides to define the expansion coefficients. As is commonly done while solving elastic problems for multiple defects, we first

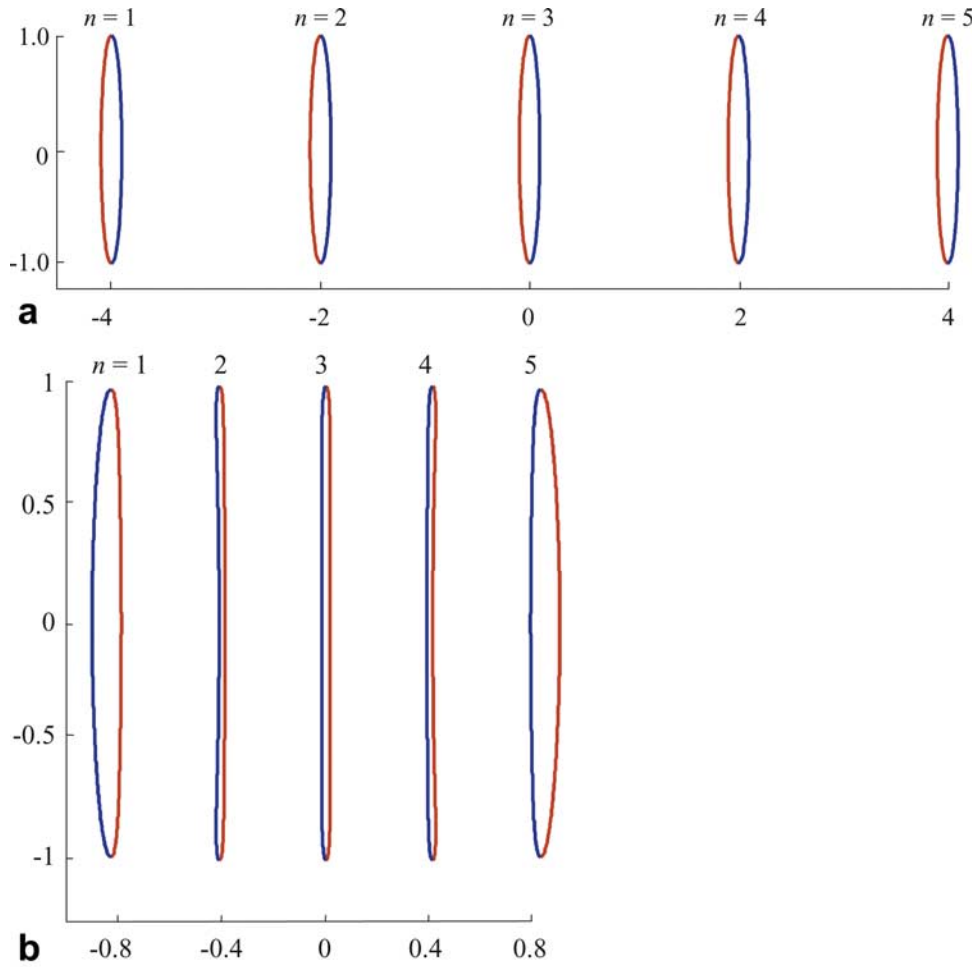

Figure 3. Openings in the set of $N = 5$ joints with different spacings: (a) $s = 1$, (b) $s = 0.2$, (c) $s = s_{cr} = 0.093$, and (d, e) $s = 0.05$. For better visualization, horizontal and vertical scales are different in Figures 3c, 3d, and 3e and all displacements/apertures are normalized by $20cp/E_1$ and shown in x/c, y/c coordinates. Figures 3d and 3e show displacements of joint sides and joint apertures for the same joint configuration. Figure 3d represents the deformed shapes of the loaded joints, which are generally not symmetric as a result of interaction. Figure 3e represents displacement discontinuities along the joints; Figure 3e is symmetric with respect to joint axes, which has little mechanical meaning but rather makes it a convenient way to visualize joint openings.

represent the problem for N interacting joints as a sum of N problems for single joints with unknown (yet to be defined) normal, s, and tangential, t, tractions on the joint sides (see Appendix A). Then, for each joint we represent the latter in the form of

$$q = s + it = -\sum_{m=1}^{M} (\alpha_m + i\beta_m) U_{m-1}(\xi) \tag{2}$$

which, after substituting into the *Muskheleshvili* [1953] potentials (see details in Appendix A), results in the displacement field,

$$\frac{4\mu}{c}(u + iv) = \sum_{m=1}^{M} \frac{\alpha_m - i\beta_m}{m} \left[-m\left(\zeta - \sqrt{\zeta^2 - 1}\right)^m + \left(\bar{\zeta} - \sqrt{\bar{\zeta}^2 - 1}\right)^m \right] - (\zeta - \bar{\zeta}) \sum_{m=1}^{M} (\alpha_m + i\beta_m) \frac{\left(\bar{\zeta} - \sqrt{\bar{\zeta}^2 - 1}\right)^m}{\sqrt{\bar{\zeta}^2 - 1}} \tag{3}$$

joint aperture,

$$W(\xi) = C\sqrt{1 - \xi^2} \sum_{m=1}^{M} \frac{1}{m} \alpha_m U_{m-1}(\xi) \tag{4}$$

and stress intensity factors,

$$K_I + iK_{II} = \sqrt{\pi c} \sum_{m=1}^{M} (\pm 1)^{m+1} (\alpha_m + i\beta_m) \tag{5}$$

Here $i^2 = -1$, $C = W_0(0) = 4c/E_1$, $E_1 = (1 - \nu^2)/E$ is the plane strain modulus, c is the joint half size (Figure 2a), $U_m(\xi) = \sin[(m + 1)\arccos(\xi)]/\sin[\arccos(\xi)]$, is the mth-order Chebyshev polynomial of the second kind, $\zeta = \xi + i\eta$ is the complex variable associated with the local coordinate set (ξ, η) of each joint, $\eta = y/c$ and $\xi = x/c$ are the local dimensionless coordinates (e.g., ξ points along x axis shown in Figure 2a), M is the number of collocation points per

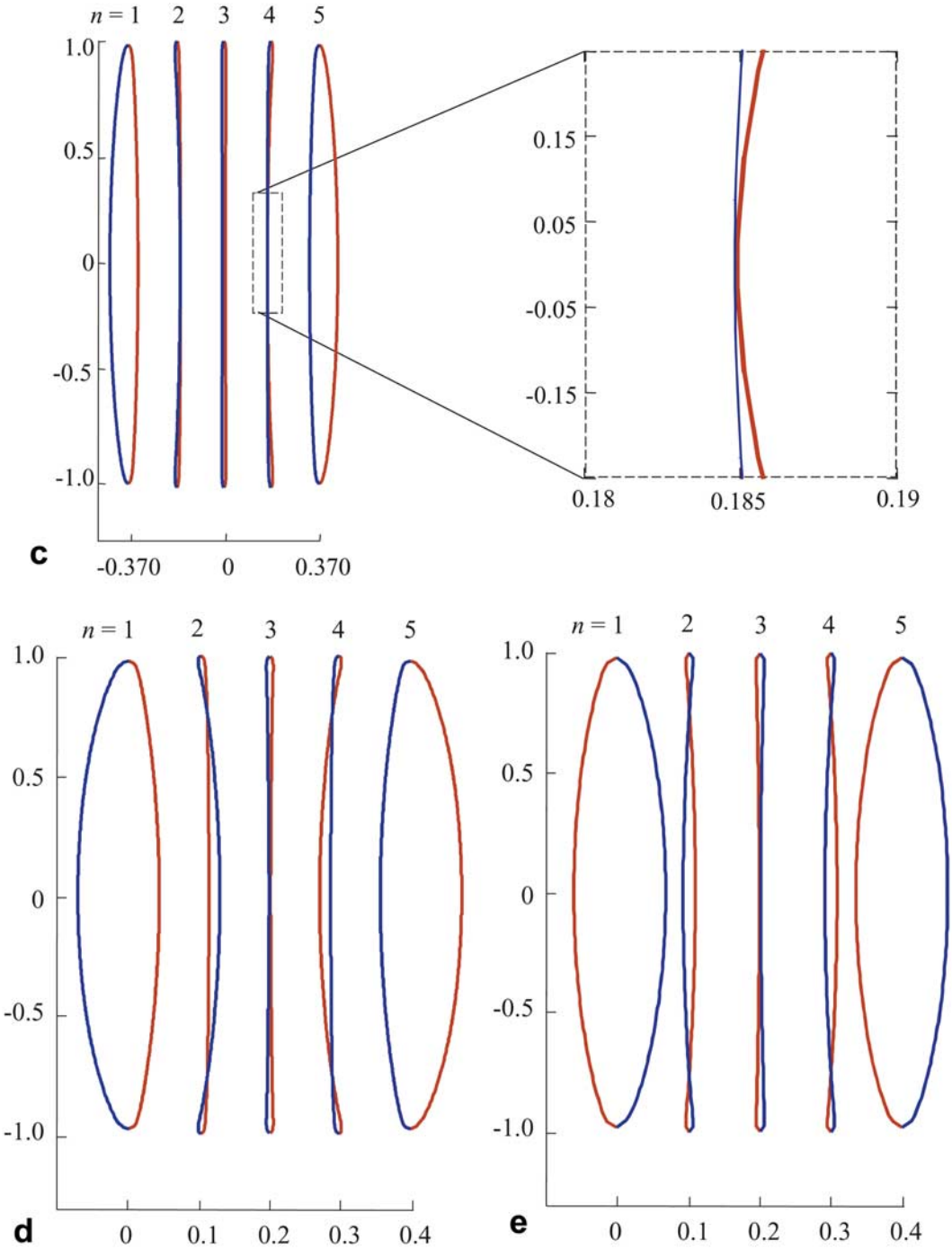

Figure 3. (continued)

joint, signs "+" and "−" correspond to the upper ($x > 0$) and lower ($x < 0$) joint ends/tips (see Figure 2a), and the coefficients, α_m and β_m, are calculated on the basis of the boundary conditions (1) on the joint sides, as described in Appendix A. Symbol definitions are also provided in the notation section.

[14] In this paper, the terms "joint", "fracture", and "crack" are identical and we use the term "opening" (as a noun) in a generic sense. Further, the term "aperture" is synonymous to "displacement discontinuity" and should be distinguished from the "opening displacement" (i.e., crack opening displacement or COD in fracture mechanics), which characterizes the deformed shape of a loaded joint (see also caption to Figure 3). If otherwise not indicated, the term "aperture" refers to the joint width at the center, e.g., $W = W(0)$ rather than $W(\xi)$. Note that while the joint aperture, given by equation (4), is independent of other joints (once coefficients α_m and β_m are known), the absolute displacement in a given point is the sum of displacements generated by each joint in this point and computed by using

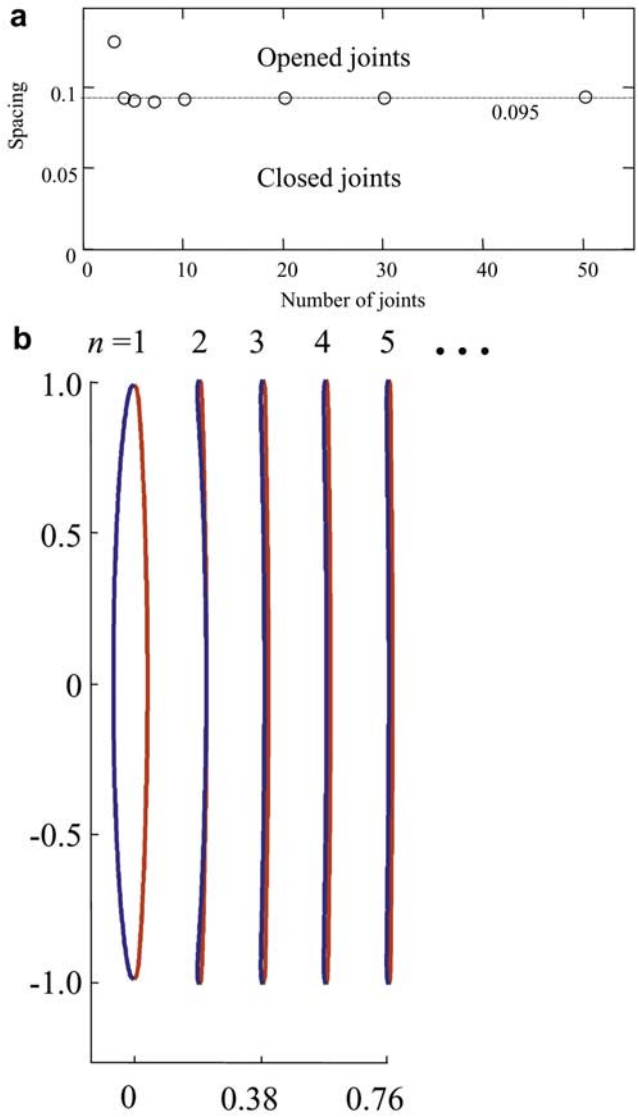

Figure 4. (a) Critical spacing, at which joint sides touch each other, as a function of the number, N, of joints in the set. (b) Opening displacements (normalized by $20cp/E_1$ and shown in x/c, y/c coordinates) in the set of $N = 50$ joints with the critical spacing, $s_{cr} = 0.095$ (joint $n = 2$ has touching sides while all other joints are opened; only the first five joints are shown to illustrate the joint openings in the semi-infinite array).

expression (3) (with a proper change of the local coordinate sets). To better visualize joint interaction, in most cases we plot both joint opening displacements and apertures.

[15] An example that demonstrates the importance of joint interaction is given in Figure 3, which shows the computed openings of five joints in the sets with different values of spacing, $s = b/(2c)$. For $s = 1$ (Figure 3a), the openings of three middle joints are only slightly smaller than the openings of two edge joints. This effect becomes more pronounced for more closely located joints ($s = 0.2$ in Figure 3b) and at a certain critical spacing, $s_{cr} = 0.093$ (Figure 3c), the sides of two internal joints adjacent to the end members (i.e., edge joints) start touching each other (enlarged in Figure 3c). For even more closely located joints, the sides start intersecting each other (Figures 3d and 3e), which is mathematically permissible since the pressure boundary conditions (1) are assigned on the joint sides. Yet penetration of joint sides through each other is physically impossible and should be interpreted as joint closure. The idea of interpenetrating joint sides is somewhat counterintuitive because joints are closing in response to the extensional load (e.g., internal pressure). Therefore we have also performed the calculations (see Appendix B) with the finite element method (FEM), which confirmed the described above results obtained by the boundary collocation technique (Appendix A). In addition, this effect has also been illustrated by a simple physical experiment described in section 4.

[16] Generally, for different number, N, of joints in the set, the joint sides begin touching at different values of $s = s_{cr}$ (Figure 4a). This critical spacing, however, remains virtually constant at $N \geq 4$ (see Figure 4a). If the distance between the joints gradually decreases (or joints become larger), the first joints with touching sides are always those adjacent to the widely open edge joints (end members), which always have the greatest aperture, $W_1 = W_1(0)$, since they are not suppressed from one side by other joints. The asymptote, $s_{cr} = 0.095$, shown in Figure 4a, apparently corresponds to the case of the semi-infinite array of joints (Figure 4b) where the second joint ($n = 2$ in Figure 4b) has touching sides while all other joints are still open (joint $n = 1$ being widely open). Similarly, if N increases while s is fixed, the aperture, $W_c = W_c(0)$, of the joints in the central region of the set should approach the aperture, $W_\infty = W_\infty(0)$, in the infinite array.

[17] Figure 5 shows the set of $N = 20$ joints with the critical spacing, $s_{cr} = 0.094$. For the values of spacing larger than s_{cr}, all joints in this set are opened (although highly unequally). If we now decrease the joint spacing, s, below the critical value, $s_{cr} = 0.094$, some joint sides start interpenetrating each other (similar to Figure 3d). Nevertheless, the asymptotic tendency of $W_c/W_\infty \to 1$ for $N \to \infty$ that was mentioned above still holds. Yet, to devise a physically meaningful model, we shall explicitly consider joints with contacting sides (see section 3). It is worth noting, however, that since in the infinite array all joints are open even for $s < s_{cr}$, in the finite set of densely located joints with a given spacing $s < s_{cr}$, the apertures of the joints located far from the set edges (i.e., far from joint $n = 1$ in Figure 4b) increase with increasing the number, N, of joints in the set. Thus there are two competing parameters affecting the aperture, W_c, of central joints, which reduces with decreasing spacing for a given N and grows with increasing N for a given joint spacing (at least for $s < s_{cr}$).

[18] In general, for each spacing and sufficiently large N, the groups of the edge and central joints can be described by the semi-infinite (Figure 4b) and infinite arrays, respectively. However, it still requires explicit calculations in every particular case of N and s to check whether or not the joints in the central and edge parts of the set can indeed be modeled by the infinite and semi-infinite sequences of cracks. For example, for the central joint in Figure 3c showing $N = 5$ joints spaced at $s_{cr} = 0.093$, $W_c/W_\infty = 1.319$, where W_∞ is the aperture of the segment in the infinite array which can be computed similarly to the

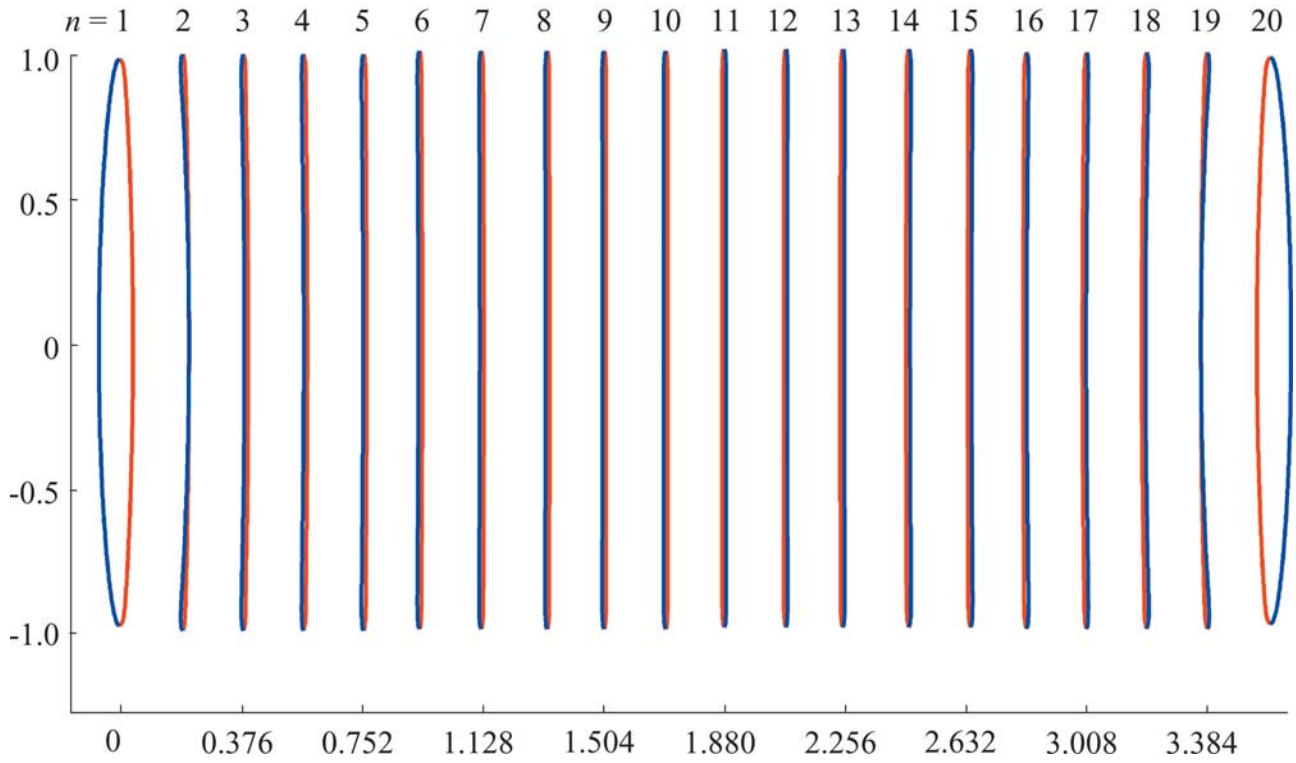

Figure 5. Opening displacements in the set of $N = 20$ joints spaced at $s = s_{cr} = 0.094$. Horizontal and vertical scales are not equal in this plot. For better visualization, displacements are normalized by $20cp/E_1$ and shown in x/c, y/c coordinates.

implemented BCM (see details in Appendix C). Maintaining practically the same spacing, $s = s_{cr} = 0.094$, and choosing $N = 20$ (Figure 5) results, however, in $W_c/W_\infty = 1.277$, which decreases to $W_c/W_\infty = 1.146$ for $N = 50$ and $s = s_{cr} = 0.095$. Note that the critical value of spacing, s_{cr}, is independent of rock elastic properties. This can clearly be seen from equation (4) where both elastic constants are combined within the factor of C and therefore zero value of displacement discontinuity is not affected by the Young's modulus and Poisson's ratio.

3. Joints With Contacting Sides

[19] As mentioned in section 2, in reality, joint surfaces cannot penetrate each other but will rather come into contact and close the joint. Because of the tensile stress concentration, the joints are not likely to become completely closed and should have some open parts adjacent to their tips (similar to the joints with interpenetrating sides considered in the previous section; e.g., see Figure 3c). Therefore it is expected that joint closure will result in a configuration similar to the one shown in Figure 6a for the set of $N = 5$ joints (only the open parts of joints are shown) and $s = 0.05$. In general, a contact problem has to be solved to confirm this expectation. Since the contacting parts of joints are not known in advance, this makes the problem nonlinear, requiring considerable calculations, usually with specially designed codes (e.g., see Appendix B).

[20] Fortunately, the boundary collocation method described above (and, with more details, in Appendix A) allows finding the end points, P and Q, of the contacting parts, PQ, of the joint sides (see Figure 6) relatively easily by assuming the smooth opening of the joint sides adjacent to the contact area, PQ. Then, using a simple condition

$$K_I = 0 \tag{6}$$

at the end points P and Q of the contact regions (Figure 6), the problem reduces to computing the elastic interaction between open parallel segments of nonequal sizes (Figure 6a). These sizes are unknown but can be computed using expression (5) for stress intensity factors and the specified condition (6). Our calculations were conducted until K_I at any segment tip, P or Q, which location we were determining (e.g., see Figure 6), became less than one percent of the smallest $K_I = K_I^{min}$ on the fixed (external) segment tips (see also Table 1). Below we reserve the term "segment" for joints or their open parts in the cases when there may be joints with contacting sides in the set. For example, as a result of closing, the set of five joints in Figure 6a becomes an arrangement of eight segments.

[21] Figure 6b shows the typical density of collocation points near the internal segment tips (the area marked in Figure 6a by the dashed rectangle) for $M = 100$. One can see that the distance between the segments is much greater than that between the collocation points on each segment. This arrangement provides excellent accuracy such that the results do not change in the fourth decimal if the number of collocation points is doubled. For better visualization of closed joints, their enlarged openings are shown in Figure 6c, which also demonstrates that K_I is negligibly

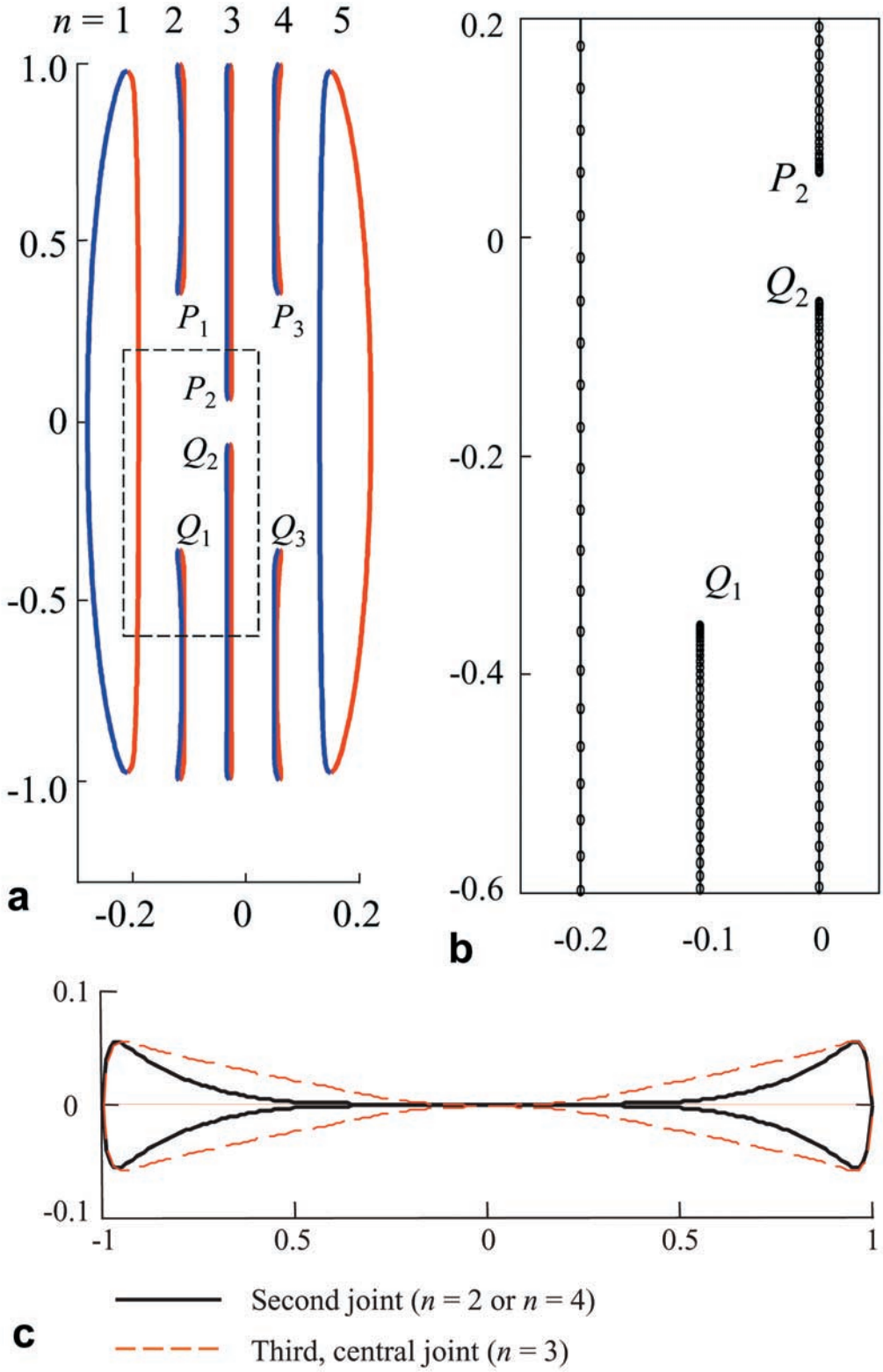

Figure 6. (a) Joint opening displacements (normalized by $20cp/E_1$) for $N = 5$ and $s = 0.05$, (b) enlarged fragment of joints with contacting sides showing collocation points, and (c) enlarged opening displacements (normalized by W_0) of the segments of the second ($n = 2$) and third ($n = 3$), partially closed joints; contacting parts of joints with zero opening are shown explicitly. Horizontal and vertical scales are different in Figures 6a and 6c. All plots are shown in x/c, y/c coordinates.

Table 1. Ratios of K_I/K_I^{min} and K_{II}/K_I^{min}, at the Tips of Segments Representing Closed Joints (Computed on the Basis of Condition (6))

Number of Joints, N	Joint Number		$n = 2$		$n = 3$		n = 4		n = 5	
	Figure	Spacing	K_I/K_I^{min}	K_{II}/K_I^{min}	K_I/K_I^{min}	K_{II}/K_I^{min}	K_I/K_I^{min}	K_{II}/K_I^{min}	K_I/K_I^{min}	K_{II}/K_I^{min}
5	6a and 6c	0.05	8×10^{-5}	1.0×10^{-2}	1.8×10^{-4}	5×10^{-6}	8×10^{-5}	1.0×10^{-2}	open	open
7	7a and 7b	0.05	2×10^{-4}	2.5×10^{-3}	6×10^{-4}	5×10^{-3}	open	open	open	open
10	7c and 7d	0.05	2.3×10^{-4}	3×10^{-3}	1.4×10^{-4}	4.3×10^{-3}	open	open	open	open
20	7e and 7f	0.05	1.0×10^{-3}	1.4×10^{-2}	1.6×10^{-3}	7.1×10^{-3}	open	open	open	open
10	8	0.02	6.7×10^{-3}	1.3×10^{-2}	6.9×10^{-3}	8.8×10^{-3}	7.8×10^{-3}	1.1×10^{-2}	2.2×10^{-3}	3.6×10^{-3}

small at the internal tips (P and Q in Figure 6a) of the open segments.

[22] As in the case of joints with interpenetrated sides (see the previous section), increasing the number, N, of joints in the set for a given spacing, s, results in the increase of the aperture of the central joints which then approaches the aperture in the infinite array with the same spacing. For example, for $N = 5$ joints spaced at $s = 0.05$ and shown in Figure 6a, $W_c/W_\infty = 0$ because the central joint is closed ($W_c = 0$). Figures 7a and 7b show displacements of joint sides and joint apertures (displacement discontinuities) in the set of $N = 7$ joints with the same spacing, $s = 0.05$. The aperture, W_c, of the central joint is small but noticable and becomes greater for equally spaced $N = 10$ joints shown in Figures 7c and 7d. The corresponding ratios, W_c/W_∞, are 0.34 and 1.44, respectively. The apertures of $N = 20$ joints with the same spacing, $s = 0.05$, are plotted in Figures 7e and 7f (compare to Figure 5). In this case, W_c/W_∞ is also 1.44 for the central joint but starts to decrease with a further increase of N ($W_c/W_\infty = 1.24$ for $N = 50$ and $s = 0.05$), indicating that $W_c/W_\infty \to 1$ as $N \to \infty$ while s is constant.

[23] Note that we normalized W_c by W_∞ to test if the central joint conditions are close to those in the infinite array. To characterize how the absolute values of joint apertures depend upon the joint set geometry, we shall use the aperture, $W_0 = W_0(0)$, of noninteracting joints of the same size, which is independent of N and s. For instance, in the case of $N = 10$ joints, obviously, $W_c/W_0 \to 1$ as $s \to \infty$ while for $N = 10$ joints (Figures 7c and 7d), W_c/W_0 reduces from 0.036 at $s = 0.05$ to 0 at $s = 0.02$ (Figure 8). Therefore decreasing the joint spacing results in reducing the joint apertures, indicating that $W_c/W_0 \to 0$ as $s \to 0$ while N is constant.

[24] Although the extremes are clear ($W_c/W_\infty \to 1$ for $N \to \infty$ and $s = \text{const}$, $W_c/W_0 \to 0$ for $s \to 0$ and $N = \text{const}$, and $W_c/W_0 \to 1$ for $s \to \infty$ and $N = \text{const}$), the parametric analysis is required to understand the intermediate cases [see *Germanovich and Astakhov*, 2004]. Nevertheless, Figures 6 through 8 confirm the peculiar effect of joint interaction described in section 2 based on the computations performed for the case of joints with overlapping (interpenetrating) sides. The effect of joint closing rather than opening as a result of applying the net (excess) pressure is not only interesting by itself, but also very important for permeability estimates of jointed, layered rock. Indeed, this effect significantly changes fracture aperture and, therefore, considerably affects permeability both quantitatively and in terms of the flow pattern (see more in the paper by *Germanovich and Astakhov* [2004]). In connection with the latter, it is worth mentioning again that the joints that are most closed are always joints $n = 2$ and $n = N - 1$ (i.e., the ones adjacent to the edge joints $n = 1$ and $n = N$), then joints $n = 3$ and $n = N - 2$ (adjacent to the most closed joints $n = 2$ and $N - 1$), etc. (see Figures 6, 7, and 8). In other words, the contact length (e.g., Figure 8) increases toward the end-member joints.

[25] In summary, the conducted analysis demonstrates that when some joints in the initial configuration are closed by the joint interaction (as in Figures 6, 7, and 8), the described above simple procedure (based on condition (6)) for computing the sizes of the open parts of each closed joint can indeed be effectively implemented. In this procedure, each closed joint is replaced by a pair of shorter segments (e.g., Figures 6a and 6c) and, accordingly, the coefficients α_m and β_m used in formulae (2), (3), (4), and (5), should be replaced by those corresponding to the new arrangement.

[26] Note that the suggested procedure generally results in $K_{II} \neq 0$ in the segment internal tips, P and Q (Figure 6). Indeed, replacing the contacting parts, PQ, of joints with the intact material prohibits both normal and shear displacement discontinuities while the absence of mode I singularity (i.e., $K_I = 0$), as specified by condition (6), does not yet guarantee that $K_{II} = 0$. From the physical standpoint, however, the method is somewhat justified by the expectation that for closely located joints loaded by the same pressure, shear displacements of contacting parts of the joint surfaces should be appreciably small. Furthermore, the natural fracture surfaces are quite likely to have considerable roughness that resists the shear along their contacting parts. Therefore it seems reasonable to assume that contacting parts of the joint are locked and cannot slip but can be opened freely. In any event, while computing (based on condition (6) of zero K_I) the locations of the closed parts of joints, we have always been checking K_{II} at the "new" (segment) tips, such as P and Q in Figure 6. Since for the considered set of parameters, the magnitude of K_{II} has never been greater than 1.5% of K_I^{min} (see Table 1), the assumptions made above appear justified.

4. Physical Experiment

[27] To demonstrate the effect of joint closure by extensional load, we conducted a simple physical experiment. For visualization purposes, five identical parallel slots, 2 mm wide and 14 cm long, were cut in a rubber sample of width and length 30.4 by 30.4 cm, and thickness 9.5 mm (neoprene spring rubber #8630K178 of durometer hardness 70A, tensile strength of 11.7 MPa and maximum elongation of 200% [see *McMaster-Carr Supply Company*, 2003, p. 3249]). The sample thickness, $h = 9.5$ mm, was sufficient to prevent the thin slabs between the slots from buckling (see below). Using considerably thicker samples did not allow the generation of sufficient displacements and, there-

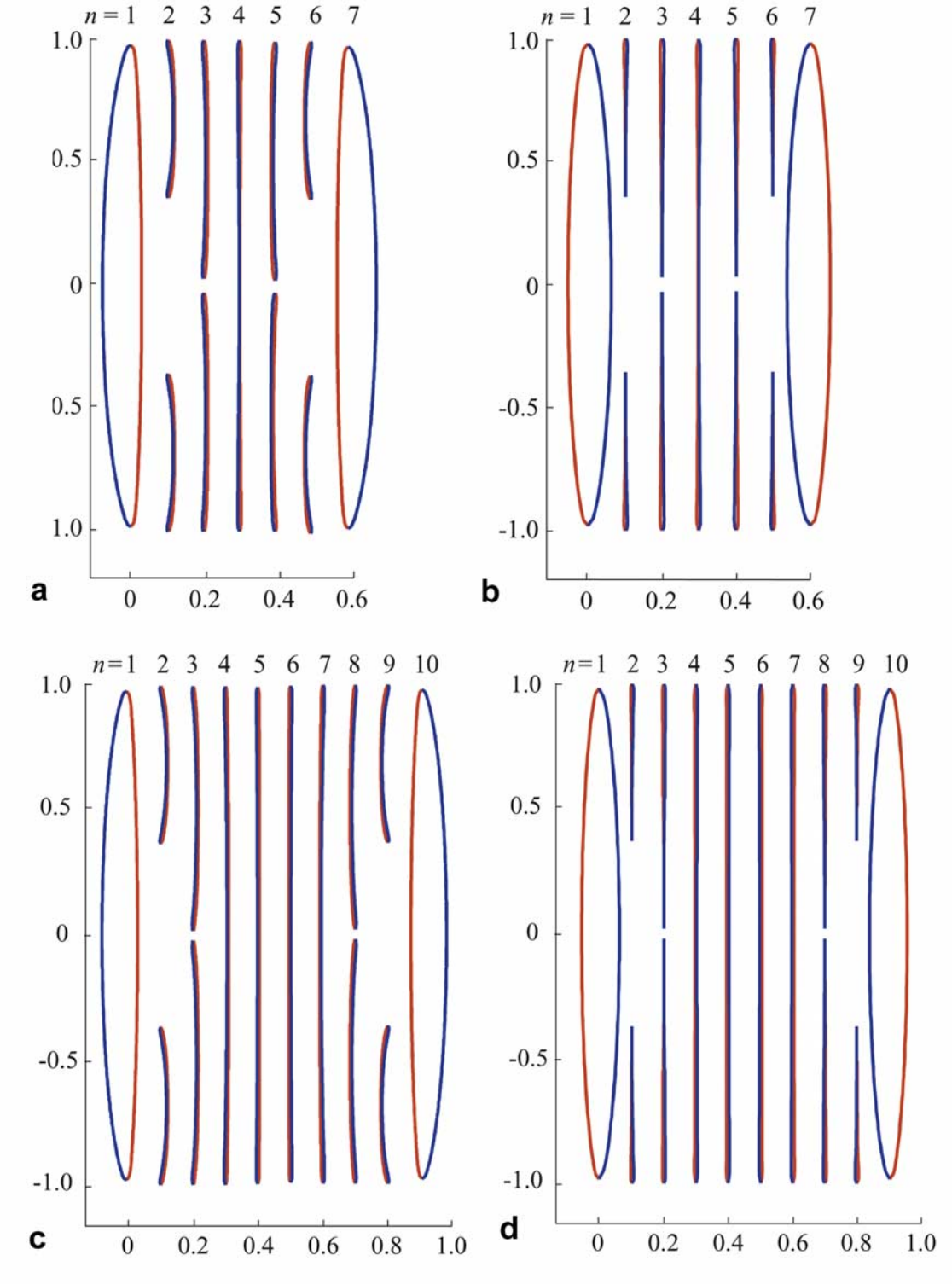

Figure 7. (a, c, e) Opening displacements and (b, d, f) displacement discontinuities in the set of $N = 7$ (Figures 7a and 7b), $N = 10$ (Figures 7c and 7d), and $N = 20$ (Figures 7e and 7f) joints spaced at $s = 0.05$. Horizontal and vertical scales for x/c and y/c are different in these plots, and all displacements/apertures are normalized by $20cp/E_1$.

fore, the slot opening/closure was not clearly visible. The sample was attached to the steel frame along its two opposing sides as shown in Figures 9a and 9b. The extensional load (in this case, displacement) was applied by translational movement of one side of the frame by turning the hand screw (see Figure 9a).

[28] Figure 9c shows the slot apertures at 10% strain applied in the direction perpendicular to the slots (Figure 9c).

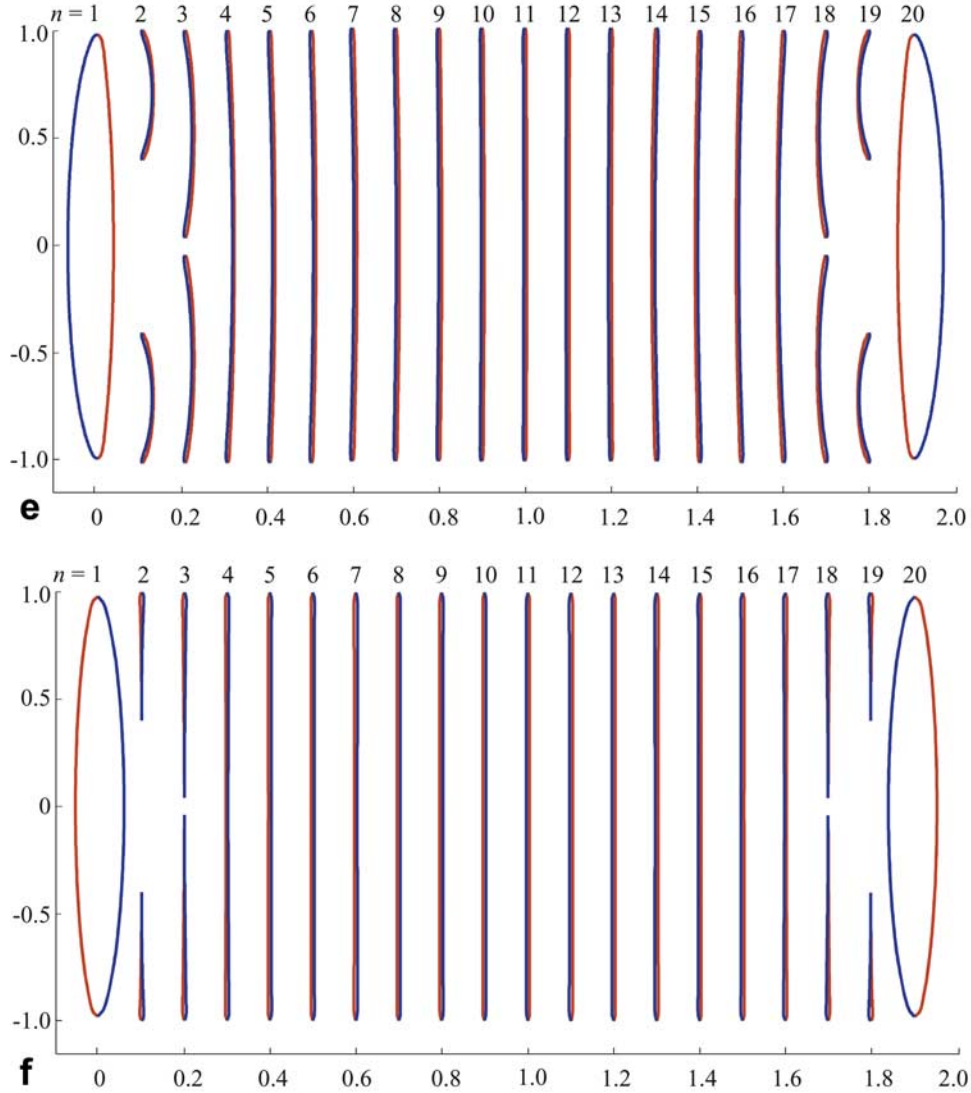

Figure 7. (continued)

It is clearly seen that while the edge slots open widely, all the internal slots close partially as a result of the extensional load. The final deformed configuration closely resembles that shown in Figure 6a. Note that we had no intention of quantitatively comparing the theoretical and experimental results because the corresponding models are rather different (i.e., infinite plane versus finite body, infinitesimally thin cracks versus finite width slots, small versus large strains, linear versus nonlinear elastic materials [e.g., *Hayden et al.*, 1965], etc.). Nevertheless, since the elastic modulus of the rubber used in the physical experiment (Figure 9) is rather low (≈3 MPa), one may argue that the slot closure could have resulted from the buckling of the thin interslot layers. This buckling may have been caused by the Poisson's effect in the direction perpendicular to the applied strain (i.e., by the compression parallel to the layers). This is why numerical modeling was conducted to quantitatively show that even rather wide slots could be closed within the linear elastic regime.

[29] Since the adopted version of the BCM does not allow the modeling of finite width slots, the FEM code FRANC2D [*Wawrzynek and Ingraffea*, 1991] was used to numerically model the physical experiment. With the exception of the rather complex material properties of rubber (see above), this allowed for a quite accurate simulation of the experimental setup and sample geometry (including the finite width slots). Because of the symmetry, only one half of the sample was simulated. Figure 10a shows the fragment of the original mesh with the slots of the same geometry as in the physical experiment. Measured values of Young's modulus ($E \approx 3.0$ MPa) and Poisson's ratio ($\nu \approx 0.45$) of the rubber material were incorporated in the numerical modeling. As in the physical experiment (Figures 9a and 9b), equal, homogeneous, extensional displacements, generating 10% overall strain, were applied to the opposing sample sides. Figure 10b shows both deformed and undeformed sample boundaries (including slots) while Figures 11a and 11b show equally scaled fragments of the physical and numerical models.

[30] One can see that the shapes of the open and partially closed segments in the physical and numerical models are quite similar. Note that the difference in slot apertures

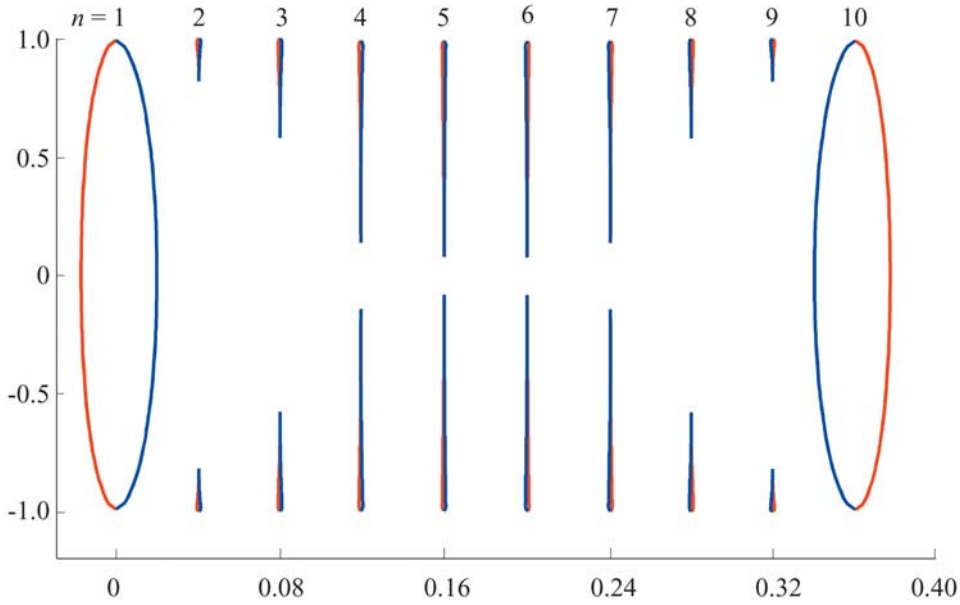

Figure 8. Apertures (normalized by $20cp/E_1$ and shown in x/c, y/c coordinates) in the set of $N = 10$ joints with contacting sides spaced at $s = 0.02$.

(approximately 35%) could be attributed to nonlinearity of the elastic properties of the rubber sample [e.g., *Hayden et al.*, 1965] and to the difference between the small strain theoretical approach adopted in FRANC2D and the large strains observed in the physical experiment. Yet, the critical force required for layer buckling can be estimated by [e.g., *Landau and Lifshitz*, 1986]

$$F_{cr} = \frac{4\pi^2 EI}{l^2}, \quad I = \min[hb^3/12,\ h^3 b/12] \tag{7}$$

where $l = 2c = 14$ cm is the layer length (twice larger than shown in Figure 11) and $b = 9.5$ mm is the layer width (same as h in the model shown in Figure 9). Expression (7) provides the estimate of 3.3 N for the buckling force, F_{cr}. The numerical model, however, results in a force of 0.16 N for the stage of deformation shown in Figure 11b. Such a difference in values most likely rules out the possibility of buckling.

[31] In addition, in the physical experiment, the layers had always deformed in plane and toward the line of symmetry (Figure 11a) while in the buckling mode, the pattern would have been random. Furthermore, since the layers in the model experiment are actually the "beams" of a square cross section (9.5×9.5 mm^2), it appears that both in-plane and out-of-plane buckling should have randomly occurred had the buckling been a deformation mechanism. In our tests, however, the out-of-plane deformation never happened, which also makes the buckling scenario rather unlikely.

[32] The numerical experiment also clarifies the mechanical reason for closing densely spaced parallel fractures, that is, the bending moment at the places of connection of the thin layers between the fractures to the reminder of the material (Figure 11).

[33] Finally, comparison with five partially closed segments (see Figure 6a) allows one to conclude that the finite width of the slots does not significantly affect the segment closure (as long as the slot widths are relatively small). Therefore the results obtained are reasonably consistent, demonstrating that the mechanical part of the developed model of stress-dependent permeability [*Germanovich and Astakhov*, 2004] is sufficiently robust.

5. Discussion

[34] The effect of joint closure under the extensional load (Figure 2b) cannot be derived from considering only stress intensity factors, K_I and K_{II}, at the joint tips where the joints are always opened (i.e., $K_I > 0$) regardless of their number and spacing (e.g., see Figures 3 and 5). *Germanovich et al.* [1998b] noticed this effect while modeling a multisegmented hydraulic fracture, which requires explicit accounting not only for fracture propagation criterion (e.g., the critical stress intensity factor, K_{Ic}), but also for fracture opening/closure that is important for addressing the fluid flow in the hydraulic fracture. Prior to their work, the elastic problem for a finite number of interacting parallel fractures had certainly been addressed in many publications [e.g., *Isida*, 1970; *Sih*, 1973; *Rooke and Cartwright*, 1976; *Theocaris and Chrysakis*, 1983; *Kishida and Asano*, 1984; *Liu and Zhou*, 1990]. Yet the effect of fracture closure had not been reported, probably because the authors were interested in the stress intensity factors rather than in the fracture apertures.

[35] *Bai and Pollard* [2001] also reported the closure of the middle fracture for $N = 3$ and $s = 0.1$. They employed a FEM and computed fracture apertures because they were studying fluid flow in parallel fractures. Since $s = 0.1 < s_{cr} = 0.129$ for $N = 3$ (Figure 4a), their result is consistent with that of *Germanovich et al.* [1998b, Figure 3], who considered the cases of $N = 3$, 7, and 11 joints, as well as with the results of this paper.

[36] *Bai et al.* [2000] also used a FEM and concluded that the aspect ratios of all but the end fractures in a

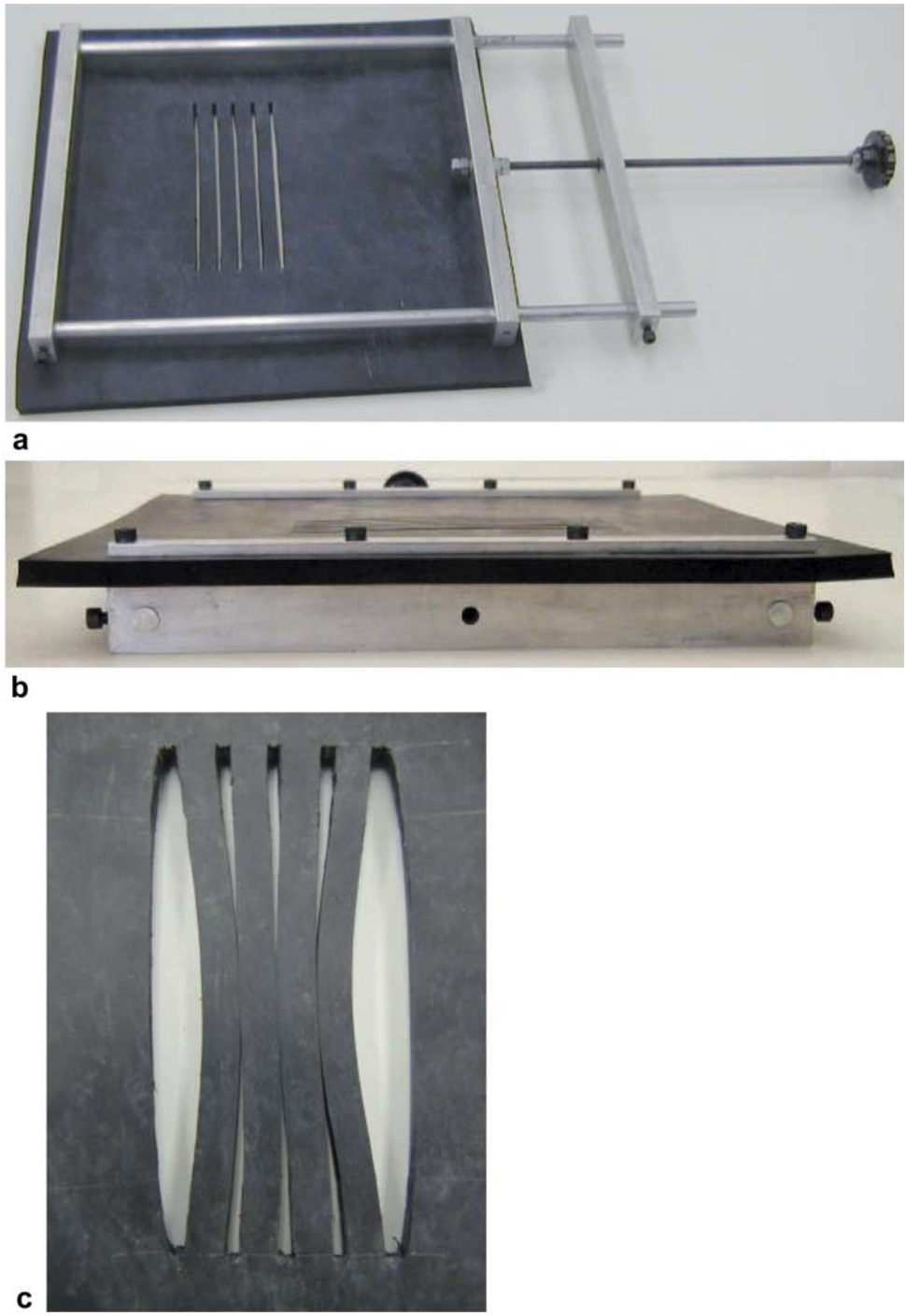

Figure 9. (a) Top and (b) side views of the experimental setup for $N = 5$ segments spaced at $s = 0.07$, and (c) segment closure as a result of the extensional load.

fracture row are very similar to each other and do not depend strongly on the number of fractures, N, in the row. On the basis of this result, they further suggested that the central fracture in the three-fracture model, that is, in the set of $N = 3$ fractures, reasonably represents fractures in a row with a larger number of fractures (i.e., with $N > 3$). Therefore they concluded that instead of calculating the aperture of each internal (confined) fracture, one could simply compute the latter in the three-fracture model (also employed by *Bai and Pollard* [2001]). This would be a significant and robust simplification compared to the accurate calculations including the ones conducted in this work. However, in the light of our results, it can now be seen that the three-fracture model can indeed be used but only if the spacing between the fractures is not too small, perhaps, if $s > 0.2 \approx 2s_{cr}$. For smaller spacing, the conclusion of *Bai et al.* [2000] that internal fractures are open approximately equally is not always valid. This can clearly be seen, for example, from Figures 7 and 8 [*Germanovich et al.*, 1998b], which illustrate that within

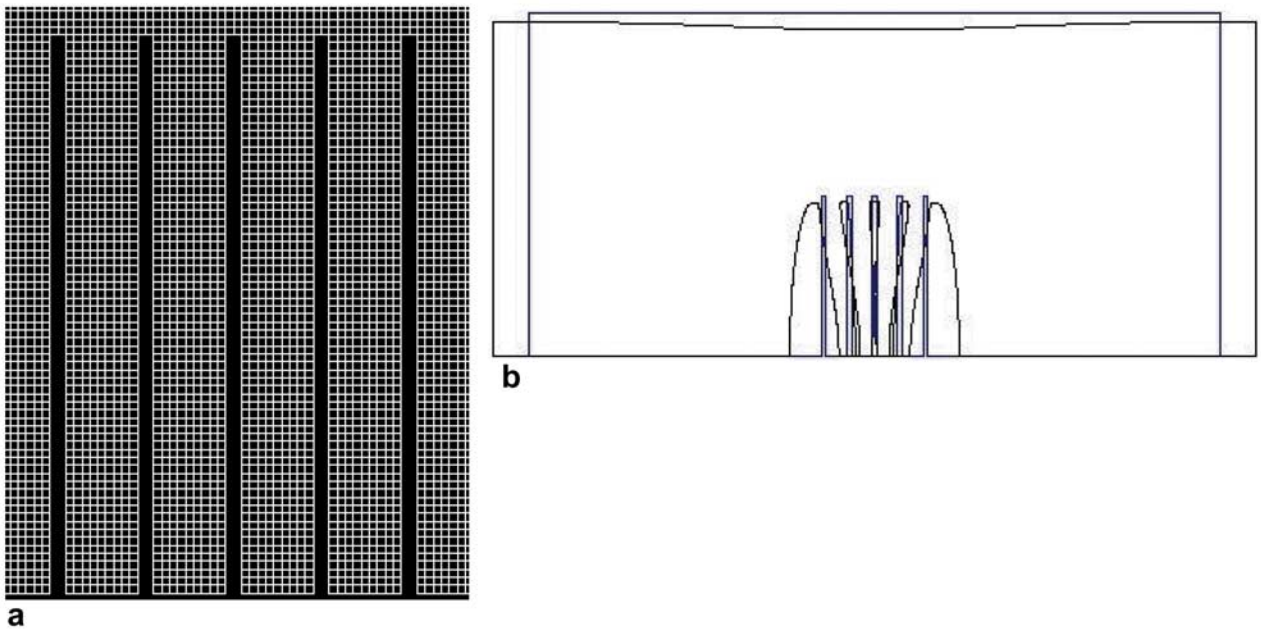

Figure 10. Finite element model of the physical experiment shown in Figure 9. (a) A fragment of the undeformed mesh with five thin slots of finite initial width. (b) Deformed and undeformed boundaries of the employed FEM model.

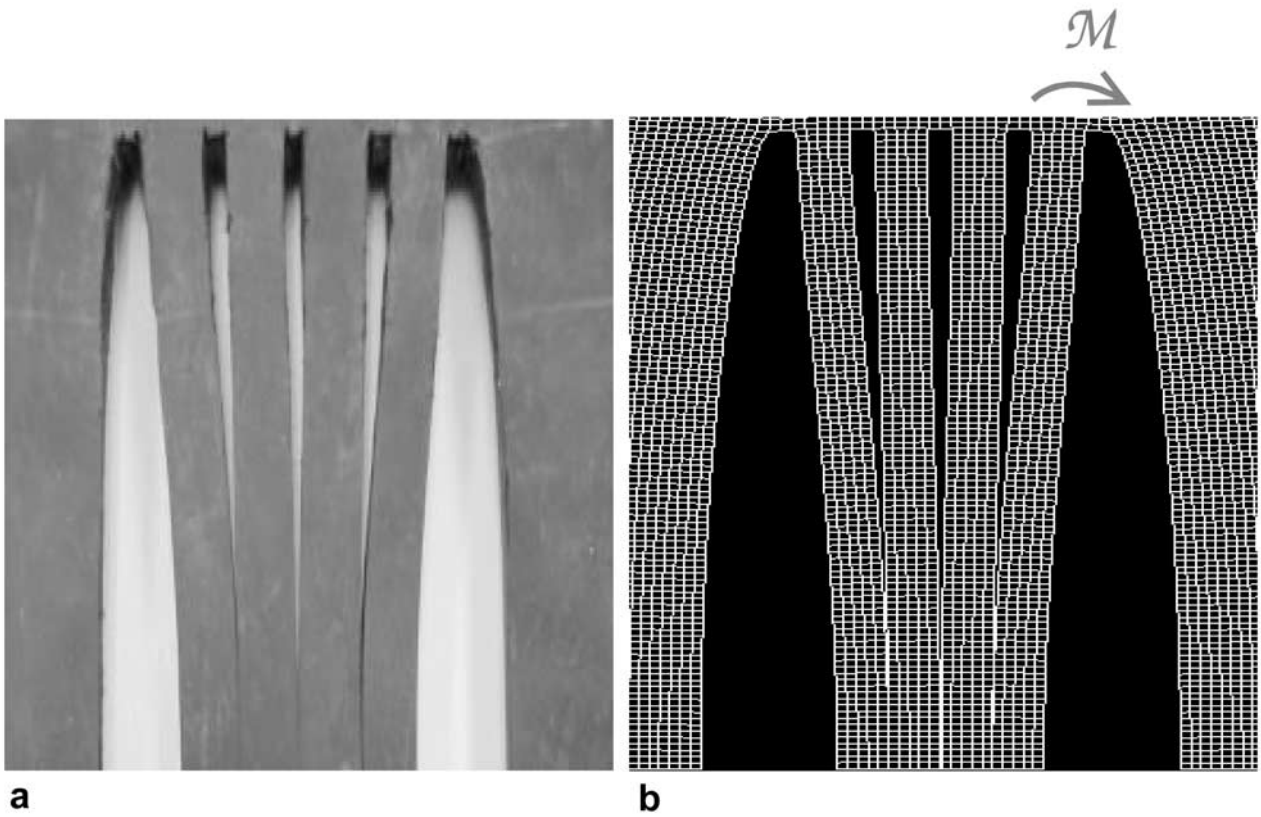

Figure 11. Fracture (slot) openings in (a) physical and (b) numerical experiments (M is the moment that bends the thin layer between the fractures, which, in turn, closes the adjacent fractures).

the same fracture set, internal members may have very different apertures, e.g., to a degree that the set can contain both closed and opened internal fractures [see also *Germanovich et al.*, 1998b, Figure 3; *Germanovich and Astakhov*, 2004, Tables 2 and 3].

[37] It is also interesting to consider the applicability of the three-fracture model to computing the apertures of the end members. Our BCM computations suggest that the difference in apertures of the end members in the cases of $N = 3$ and $N > 3$ does not exceed 20% [see also *Germanovich and Astakhov*, 2004, Figure 4a]. Furthermore, this difference asymptotically tends to zero as $s \to 0$. Therefore, although it appears that the three-fracture model approximates the apertures of the end members fairly well, the model is to be employed with some caution since the results obtained for internal (middle) members are reasonably accurate only for sufficiently large s, e.g., $>2s_{cr}$. We have not implemented this model because we had a rather accurate computational technique, that is, BCM, available (Appendix A) for sufficiently large and dense sets of fractures.

6. Conclusions

[38] We have considered parallel joint sets that represent one of the typical pathways for fluid flow in sedimentary rocks. It is well known that in many cases rock permeability depends upon the in situ stress conditions and on the pressure of the flowing fluid. Frequently, joint sets are closely spaced and although joint mechanical interaction could significantly affect their aperture, the interaction is usually ignored in the evaluation of permeability. On the basis of conducted computations and physical experiments, we suggest that the internal pressure or extensional load can, in fact, close the pressurized joints. In general, there is a critical spacing ($s \approx 0.95$ for $N \geq 4$) between the parallel fractures below which their surfaces start to contact each other under the extensional load, dramatically reducing rock permeability. However, two edge fractures in the set remain widely open because they are not suppressed from one side. As a result [see *Germanovich and Astakhov*, 2004], unless the number of joints in the set is exceedingly large (typically, $>10^3$), the fluid flow through the joint set becomes highly heterogeneous, focusing in the end members (edge joints).

Appendix A

[39] The boundary collocation method (BCM) consists of employing an exact series solution to the governing differential equations, truncating these series to a finite number of terms, and defining the unknown series coefficients by satisfying the boundary conditions (i.e., equation (1) in our case) not exactly but in a number of collocation points. The idea of the BCM version employed in this work can be illustrated with the example of two cracks, L_1 and L_2, located in an infinite plane and loaded by tractions $p_1 = \sigma_1 + i\tau_1$ and $p_2 = \sigma_2 + i\tau_2$ (Figure A1), where σ and τ are normal and tangential traction components, respectively.

[40] As is well known, such a problem can be represented as a sum of two auxiliary problems for single cracks in an infinite plane (Figure A1). In each of these problems, the cracks are loaded by unknown tractions, $q_1(z_1) = s_1(z_1) + it_1(z_1)$ and $q_2(z_2) = s_2(z_2) + it_2(z_2)$, where $z_1 = x_1 + iy_1$ and $z_2 = x_2 + iy_2$ are the local coordinates (Figure A1) attached to the first and second crack, accordingly. For each auxiliary problem, we calculate the stresses, $\Delta q_1 = \Delta s_1 + i\Delta t_1$ and $\Delta q_2 = \Delta s_2 + i\Delta t_2$, created by each crack at the location of the other one (inclined at the angle of θ to the first crack):

$$\Delta q = \Phi(z) + \overline{\Phi(z)} + e^{2i\theta}\left[\overline{\Phi(\bar{z})} - \Phi(z) - (z-\bar{z})\Phi'(z)\right], \quad \text{(A1)}$$

where the complex potential, $\Phi(z)$, can be represented in the coordinates, z, associated with the crack by [*Muskhelishvili*, 1953]

$$\Phi(z) = \frac{1}{2\pi\sqrt{z^2-c^2}} \int_{-c}^{c} \frac{\sqrt{c^2-t^2}}{t-z}\overline{q(t)}dt. \quad \text{(A2)}$$

Substituting representation (2) into (A2) and employing Gauss-Chebyshev integration rule [e.g., *Gladwell and England*, 1977]

$$-\frac{1}{\pi}\int_{-1}^{1} \frac{\sqrt{1-\xi^2}}{\xi-\zeta}U_{m-1}(\xi)d\xi = \left[\zeta - \sqrt{\zeta^2-1}\right]^m, \quad |\xi| < 1, \quad m \neq 0 \quad \text{(A3)}$$

we have for the *Muskhelishvili* [1953] potential

$$\Phi(\zeta) = \frac{1}{2\sqrt{\zeta^2-1}} \sum_{m=1}^{M} (\alpha_m - i\beta_m)\left[\zeta - \sqrt{\zeta^2-1}\right]^m \quad \text{(A4)}$$

where $\zeta = z/c$.

[41] Therefore we conclude, on the basis of (A1), that the auxiliary stresses, Δq, are also linearly expressed through the same coefficients, α_m and β_m. Since the sum of the solutions of the auxiliary problems gives the tractions in the original problem, that is,

$$q_1(z_1) + \Delta q_2(z_1) = p_1, \quad q_2(z_2) + \Delta q_1(z_2) = p_2 \quad \text{(A5)}$$

we arrive at the system of $2M$ algebraic equations for $2M$ unknown complex coefficients, $\alpha_m^1 + i\beta_m^1$ and $\alpha_m^2 + i\beta_m^2$, describing, according to equations (3), (4) and (5), crack openings and stress intensity factors.

[42] Similarly, in the case of N cracks in an infinite plane, N auxiliary problems for N single cracks can be considered so that system (A5) will consist of N complex equations. If each equation is satisfied in M collocation points on each crack, we arrive at the system of $2MN$ linear algebraic equations for unknown real coefficients. In a slightly more general case, the number of collocation points, M, can vary from crack to crack and the cracks do not necessarily need to be parallel and/or have the same sizes.

[43] Thus a system of linear algebraic equations with respect to α_m^s and β_m^s ($m = 1, \ldots, M_s$, $s = 1, \ldots, N$) can be obtained as a result of employing the BCM described above. Here we express this system in a convenient form suggested

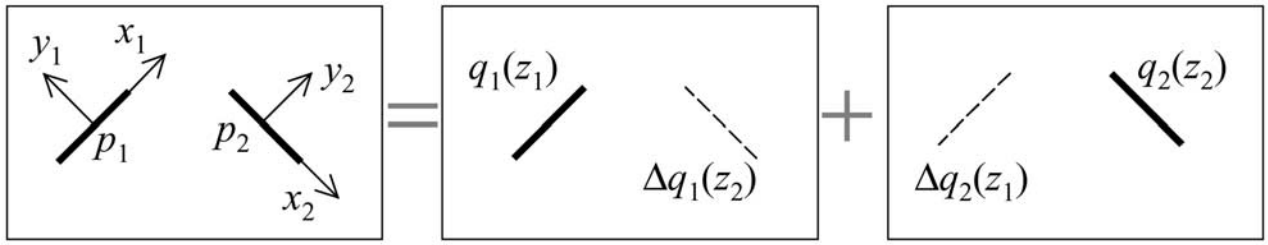

Figure A1. Original and auxiliary problems for interacting cracks.

by *McCartney and Gorley* [1987] and slightly modified here:

$$-\sum_{m=1}^{M_s}\left(\alpha_m^s+i\beta_m^s\right)U_{m-1}\left(z_s^j\right)+\sum_{\substack{r=1\\ r\neq s}}^{N}\sum_{m=1}^{M_r}\left\{\alpha_m^r I_m^r\left(z_s^j\right)+\beta_m^r J_m^r\left(z_s^j\right)\right\}$$
$$+\sum_{\substack{r=1\\ r\neq s}}^{N}e^{2i(\theta_r-\theta_s)}\left[\sum_{m=1}^{M_r}\beta_m^r\left\{iI_m^r\left(z_s^j\right)-J_m^r\left(z_s^j\right)\right\}\right.$$
$$\left.+\sum_{m=1}^{M_r}\left(\alpha_m^r-i\beta_m^r\right)\left\{K_m^r\left(z_s^j\right)+iL_m^r\left(z_s^j\right)\right\}\right]$$
$$=\sigma_s\left(z_s^j\right)-\sigma_\infty+i\left[\tau_s\left(z_s^j\right)-\tau_\infty\right]$$
$$\left(j=1,\ldots,M_s,\ s=1,\ldots,N\right) \qquad \text{(A6)}$$

The first sum in equation (A6) represents the unknown tractions, q_s, on the sth crack (compare to equations (2) and (A5)) while other sums give the additional traction, Δq_s, accounting for the interaction (see also Figure A1 and equation (A5)); $p_s = \sigma_s + i\tau_s$ are the external tractions applied to the sides of the sth crack; $p_\infty = \sigma_\infty + i\tau_\infty$ is the remote load in the local coordinates, $\zeta_s = \xi_s + i\eta_s$, associated with the sth crack; $z_s^j = x_s^j + iy_s^j$ are the sets of discrete (collocation) points (in the global coordinates $z = x + iy$) on the cracks at which the boundary conditions should be satisfied exactly; and functions I_m^r, J_m^r, K_m^r, and L_m^r are defined by

$$I_m^r(z)\ +iJ_m^r(z)=\frac{G_m(\zeta_r)}{\sqrt{\zeta_r^2-1}},$$
$$K_m^r(z)+iL_m^r(z)=\frac{1}{2}\left(\zeta_r-\bar{\zeta}_r\right)\left[\frac{m}{\sqrt{\zeta_r^2-1}}+\frac{\zeta_r}{\zeta_r^2-1}\right]\frac{G_m(\zeta_r)}{\sqrt{\zeta_r^2-1}} \qquad \text{(A7)}$$
$$\zeta_r=\frac{2z-t_1^r-t_2^r}{t_2^r-t_1^r},$$
$$G_m(\zeta_r)=\left[\zeta_r-\sqrt{\zeta_r^2-1}\right]^m,\quad m\geq 1$$

where t_1^r and t_2^r are the complex coordinates of the tips of the rth crack in the global coordinate system (x, y) while θ_r is the rth crack inclination to the x axis (so that the length of the rth crack is $2c_r = |t_1^r - t_2^r|$). The collocation points, z_s^j, can be chosen arbitrary but those based on the roots of Chebyshev's polynomials,

$$z_s^j=x_s^j+iy_s^j=\frac{1}{2}\left(t_2^s-t_1^2\right)+\frac{1}{2}\left(t_2^s-t_1^s\right)\cos\frac{\pi(2j-1)}{2M} \qquad \text{(A8)}$$

provide the fastest convergence of the adopted Chebyshev's series [e.g., *Demidovich and Maron*, 1987].

[44] Solution of the system (A6) gives the coefficients α_m and β_m for each crack (we further omit the subscripts and superscripts s for the sth crack to simplify the notations). Then, in the local coordinate system, ζ, the displacement discontinuity normal to the crack surface and the stress intensity factors are given by expressions (4) and (5),

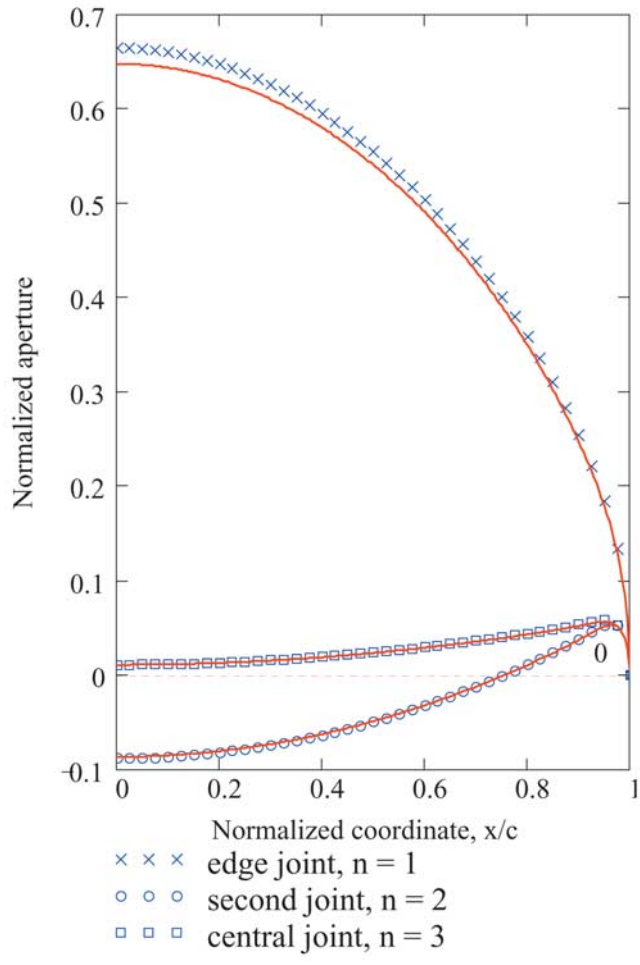

Figure B1. Normalized apertures, $W(\xi)/W_0$, of the edge and internal joints in the set of $N = 5$ joints spaced at $s = 0.05$. The curves and symbols show the results obtained by BCM and FEM, respectively. Because of the symmetry of the set, the plots for joints $n = 1$, $n = 2$ are identical to those for joints $n = 5$, $n = 4$, respectively.

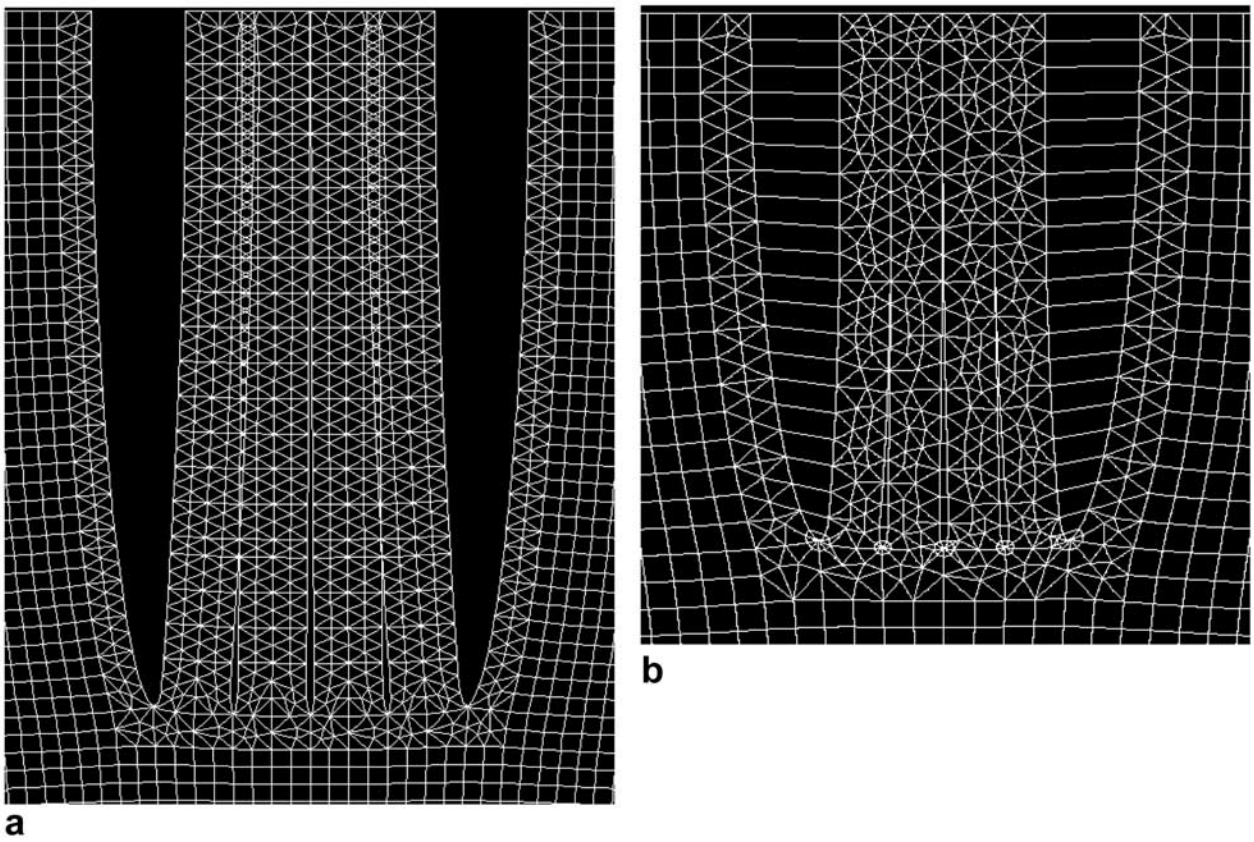

Figure B2. Fragments of the deformed FEM mesh. (a) Traction boundary conditions (1) on the joint sides (allowing their interpenetration); the built-in option of the Gaussian elimination method was used for analysis in FRANC2D. (b) Boundary condition of nonpenetrating segment sides modeled by the gap elements in FRANC2D; the built-in option of the dynamic relaxation method of analysis was used in FRANC2D (the parameter of crack side interference was set to 0.01, while the unbalanced residual load was set to 10^{-5} of the initial load).

respectively [e.g., *McCartney and Gorley*, 1987]. The area of crack opening can be found by integrating equation (4) along the joint:

$$S = c\int_{-1}^{1} W(\xi)d\xi = cC\sum_{m=1}^{M}\frac{1}{m}\alpha_m\int_{-1}^{1}\sqrt{1-\xi^2}\,U_{m-1}(\xi)\,d\xi = \frac{\pi}{2}cC\alpha_1 \tag{A9}$$

[45] In the case considered in this work, $\sigma_s = -p$ and $\tau_s = 0$ are the same for all cracks (compare to equation (1)) and so are crack inclinations [$\theta_1 = \theta_2 = \ldots = \theta_N$]. The system (A6) is solved using the standard Gaussian elimination algorithm.

Appendix B

[46] The tendency of densely located joints to close in response to the extensional load has also been checked by the numerical code FRANC2D [*Wawrzynek and Ingraffea*, 1991] which is based on the finite element method (FEM). An example of "openings" in the set of five joints computed by the boundary collocation method (Appendix A) using the traction boundary conditions (1) is shown in Figure B1 by curves for joint spacing, $s = 0.05$. A fragment of the FRANC2D deformed mesh for five joints is shown in Figure B2 (the total model size exceeds that of the shown fragment by more than a factor of 20). FRANC2D results are also plotted in Figure B1 using symbols. The discrepancy between the FEM and BCM results is no greater than 2.5% for the most opened (edge) joint while for the internal (suppressed and closed) joints, it is not greater than 0.1%. Even though such a disagreement is acceptable, it is worth noting that in this particular case, the results obtained by the boundary collocation method seem to be more accurate since they do not change in the fourth decimal when the number of collocation points per joint varies from $M = 100$ to $M = 200$. Similar agreement was obtained for the sets of $N = 3$ and $N = 7$ joints.

[47] For modeling cracks with contacting sides, FRANC2D has a gap element option that allows assigning the condition of nonpenetration of the crack sides and, therefore, the determination of the partial contact between the crack surfaces via the built-in iteration procedure [*Wawrzynek and Ingraffea*, 1991]. Because of the somewhat counterintuitive nature of the results obtained by the BCM, it was appealing to have an independent, FEM check for densely located closed joints, that is, with

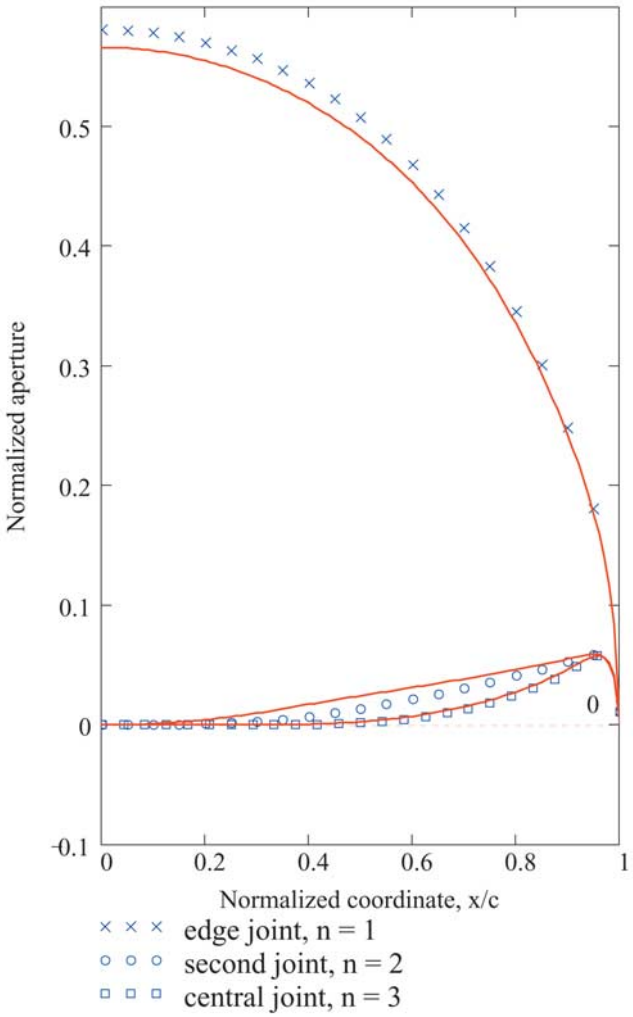

Figure B3. Normalized apertures, $W(\xi)/W_0$, of the edge and internal joints (with contacting sides) in the set of $N = 5$ joints. The curves and points show the results obtained by BCM and FEM, respectively. Similar to Figure B1, because of the symmetry, the plots for joints $n = 1$, $n = 2$ are identical to those for joints $n = 5$, $n = 4$, respectively.

contacting sides, (at least for a small N). Figure B2b shows the fragment of FRANC2D mesh with nonpenetrating segment sides (joints are modeled by the gap elements). Figure B3 compares the results obtained with FRANC2D and by the boundary collocation method (Appendix A).

Appendix C

[48] The problem of the infinite periodic array of interacting cracks (Figure C1) has become rather classic [e.g., see *Benthem and Koiter*, 1973; *Delameter et al.*, 1975] and is presented in most handbooks on stress intensity factors [e.g., *Sih*, 1973; *Rooke and Cartwright*, 1976; *Tada et al.*, 1985; *Murakami*, 1987]. However, except for the approximate approach of *Bai et al.* [2000] (see discussion in section 4), we are not aware of published studies presenting the computed openings of cracks in the infinite periodic array. Here we briefly describe how the openings were computed in this work.

[49] In the case of the infinite periodic array of joints (Figure C1), the opening of each joint can be described by the same singular integral equation [e.g., *Panasyuk et al.*, 1977]:

$$\int_{-1}^{1} \left[g'(\xi) K(\xi - \eta) + \overline{g'(\xi)} L(\xi - \eta) \right] d\xi = \pi p(\eta) c, \quad |\eta| < 1 \quad \text{(C1)}$$

where

$$K(\tau) = \frac{\pi\lambda}{2} \mathrm{Re}\left[e^{i\beta} \cot \frac{\pi\lambda\tau e^{i\beta}}{2} \right] \quad \text{(C2)}$$

is the singular kernel of the Cauchy type [because $\cot z = 1/z + O(z)$, $z \to 0$];

$$L(\tau) = \frac{\pi\lambda}{4} \left(e^{-i\beta} - e^{-3i\beta} \right) \left[\cot \frac{\pi\lambda\tau e^{-i\beta}}{2} - \frac{\pi\lambda\tau e^{-i\beta}}{2} \left(\mathrm{cosec} \frac{\pi\lambda\tau e^{-i\beta}}{2} \right)^2 \right] \quad \text{(C3)}$$

is the regular kernel [since $\cot z - z\mathrm{cosec}^2(z) = O(z)$, $z \to 0$];

$$g'(\xi) = \frac{2G}{1+\kappa} \frac{d}{d\xi} (W - iU) \quad \text{(C4)}$$

is the unknown density of displacement discontinuity, $W - iU$; $\tau = \xi - \eta$; β is the angle between the array direction and the segment orientation (Figure C1); W and U are the normal and shear displacement discontinuities, respectively; G is the shear modulus; $\kappa = 3 - 4\nu$ for plain strain condition (under consideration); ν is the Poisson's ratio; and $\lambda = 2c/d$ is the dimensionless segment size. The Gauss-Chebyshev method [e.g., *Erdogan et al.*, 1973] employed in Appendix A is also readily available to

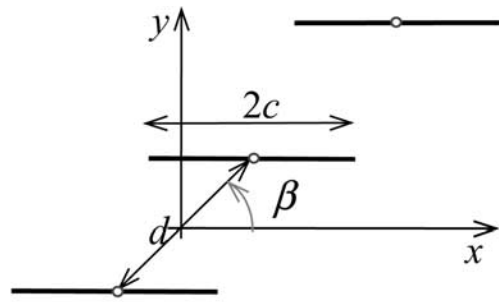

Figure C1. Infinite periodic array (en echelon) of joints. The case of parallel joints corresponds to $\beta = \pi/2$.

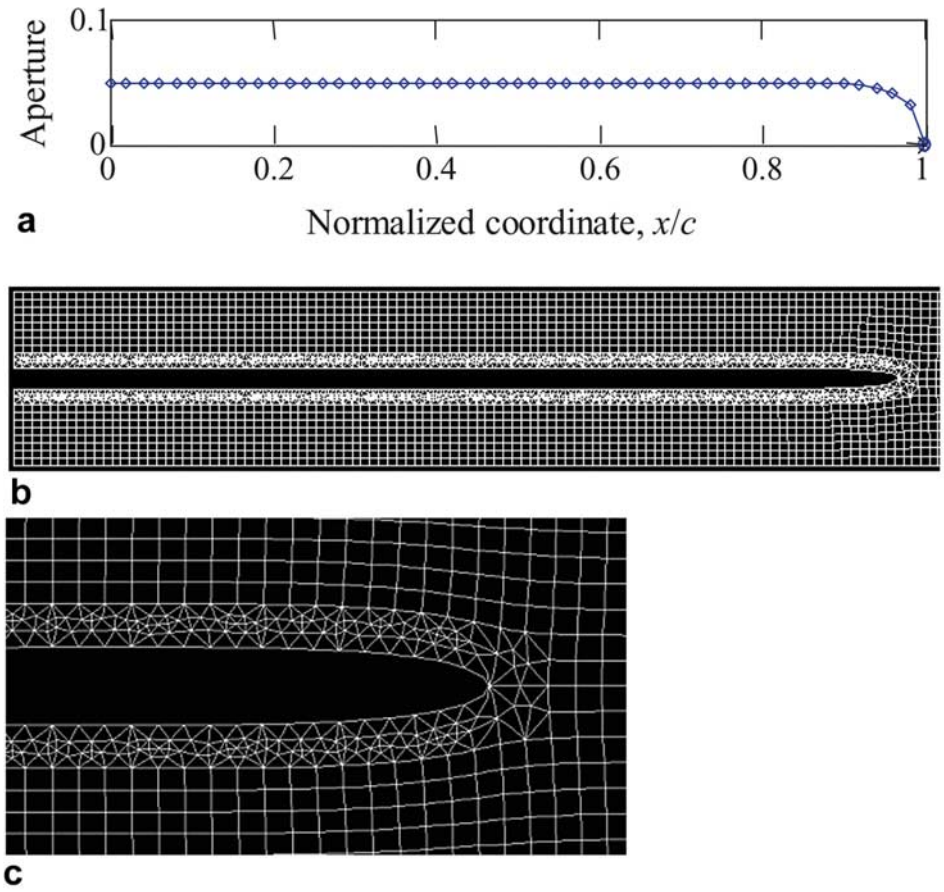

Figure C2. (a) Normalized aperture, $W_\infty(\xi)/W_0$, of segments in the infinite array obtained by BCM (lines) and FEM (diamonds) for $s = 0.05$, (b) the deformed FEM mesh (FRANC2D) for the same array modeled in a symmetry cell (strip), and (c) a fragment of this mesh showing the details near the fracture tip and crack sides.

integrate equation (C1) numerically, which should be done together with the condition

$$\int_{-1}^{1} g'(\xi)d\xi = 0 \tag{C5}$$

of displacement single-valuedness (guaranteeing that equation (C1) has a unique solution).

[50] Taking into account that $g'(\xi)$ can be further represented as [e.g., *Muskhelishvili*, 1992]

$$g'(\xi) = \varphi(\xi)/\sqrt{1-\xi^2} \tag{C6}$$

where $\varphi(\xi)$ is a bounded function, we arrive at the system [e.g., *Erdogan and Gupta*, 1972; *Savruk*, 1981]

$$\frac{1}{M}\sum_{k=1}^{M}[\varphi_k K(\xi_k-\eta_m)+\overline{\varphi_k}L(\xi_k-\eta_m)] = \pi p(\eta_m)c \quad (m=1,2,\ldots,M-1)$$
$$\sum_{k=1}^{M}\varphi_k = 0. \tag{C7}$$

of M linear algebraic equations with M unknowns, $\varphi_k = \varphi(\xi_k) = g'(\xi_k)\sqrt{1-\xi_k^2}$. Here

$$\eta_m = \cos\frac{\pi m}{M} \quad (m=1,2,\ldots,M-1),$$
$$\xi_k = \cos\frac{\pi(2k-1)}{2M} \quad (k=1,2,\ldots,M) \tag{C8}$$

are the roots of the Chebyshev polynomials of the second, $U_{M-1}(\eta)$, and first, $T_M(\xi)$, kind, respectively.

[51] After solving this system for $\beta = \pi/2$ and $p(\eta_m) = -p$, where p is the constant net pressure that opens the joints (compare to equation (1)), the distribution of the displacement discontinuities along the joint sides can be found from equation (C4):

$$W(\xi) - iU(\xi) = -\frac{1+\kappa}{2G}\int_{\xi}^{1} g'(\eta)d\eta \tag{C9}$$

where $g'(\xi)$ is expressed through $\varphi(\xi)$ by equation (C6). Since at this stage, $\varphi(\xi)$ is already known in the collocation points, ξ_k, given by equation (C8), this bounded function

can be represented employing the Lagrange interpolation formula [e.g., *Panasyuk et al.*, 1977]:

$$\varphi(\xi) = \frac{1}{M}\sum_{k=1}^{M}\varphi_k\left[-1 + 2\sum_{m=0}^{M-1}T_m(\xi_k)T_m(\xi)\right] = \frac{2}{M}\sum_{k=1}^{M}\varphi_k\sum_{m=1}^{M-1}T_m(\xi_k)T_m(\xi) \tag{C10}$$

where we used the second expression in the equation set (C7) and that $T_0(\xi) \equiv 1$ [e.g., *Korn and Korn*, 2000]. Taking into account that $T_m(\xi) = -(1/m)(1 - \xi^2)^{1/2}d[\sin(m\arccos\xi)]/d\xi$ [e.g., *Korn and Korn*, 2000, equations (21.7–3) and (21.7–4)] we have

$$\int_{\xi}^{1}\frac{T_m(t)dt}{\sqrt{1-t^2}} = \frac{1}{m}\sin(m\arccos\xi) = \frac{1}{m}U_{m-1}(\xi)\sqrt{1-\xi^2} \qquad (m = 1, 2, \ldots) \tag{C11}$$

which, after inserting equations (C6), (C10), and (C11) into equation (C9), finally results in

$$W(\xi) - iU(\xi) = -\frac{1+\kappa}{G}\frac{1}{M}\sqrt{1-\xi^2}\cdot\sum_{k=1}^{M}\varphi_k\sum_{m=1}^{M-1}T_m(\xi_k)\frac{1}{m}U_{m-1}(\xi) \tag{C12}$$

Using equation (C12) for numerical integration in equation (C9) represents no difficulty. An example is shown in Figure C2a and compared to the FEM calculations (Figures C2b and C2c). Note that except a small region around the tip, the crack sides are practically parallel. *Germanovich and Astakhov* [2004] use this circumstance for asymptotic analysis of apertures of parallel joints in the infinite set.

Notation

b	distance between joints (Figure 2).
c	joint half-size (Figure 2).
$C = W_0(0)/p = 4c(1-\nu^2)/E$	aperture of a single joint loaded by the unit pressure.
$d = b/\sin\beta$	distance between joint centers (Figure C1).
E	Young's modulus.
$E_1 = E/(1-\nu^2)$	plane strain modulus.
$g'(\xi)$	derivative (C4) of normalized displacement discontinuity (dislocation density).
G	shear modulus.
$i = \sqrt{-1}$	imaginary unit.
$K(\tau)$	singular kernel (C2) of the Cauchy type in (C1) .
$K_I^{\min}$	smallest K_I at the external tips of segments.
$L(\tau)$	regular kernel (C3) in (C1).
L	lateral dimension of the joint set (Figure 2a).
L_p	spatial scale of pressure change along z direction.
M	number of collocation points.
N	number of joints in a set.
p_i	pressure inside joints (Figure 2b).
$p = p_i - \sigma_\infty$	net pressure inside joints (Figure 2b).
$p(z) = \sigma(z) + i\tau(z)$	external tractions applied to the crack sides.
P	geometrical point of a tip of internal segment.
$q(z) = s(z) + it(z)$	unknown complex tractions applied to the crack sides in (A2) and (A5).
Q	geometrical point of a tip of internal segment.
$s = b/(2c)$	normalized joint spacing.
s_{cr}	critical joint spacing at which joint sides start touching.
$s(z)$	normal unknown traction applied to the sides of the crack (Appendix A).
S	area (A9) of crack opening.
t	real coordinate along the crack in auxiliary problem (e.g., in (A2)).
$t(z)$	tangential unknown traction applied to the crack sides (Appendix A).
T_m	mth-order Chebyshev polynomial of the first kind.
$u + iv$	displacement field.
U	shear displacement discontinuity.
U_m	mth-order Chebyshev polynomial of the second kind.
$W(x)$	displacement discontinuity or aperture.
$W_0(x)$	aperture of a single joint.
$W_0 = W_0(0)$	aperture of a single joint in the center.
$W_n(x)$	aperture of the nth joint.
$W_n = W_n(0)$	aperture of the nth joint in the center.
$W_c(x)$	aperture of the central joint.
$W_c = W_c(0)$	aperture of the central joint in the center.
$W_\infty(x)$	aperture of a joint in the infinite array.
$W_\infty = W_\infty(0)$	aperture of a joint in the infinite array in the center.
x, y, z	coordinate system aligned with the joint (Figure 2a).
$z = x + iy$	complex coordinate (used the in appendixes).
α_i, β_i	coefficients of Chebyshev polynomial series expansion.
β	angle between the array direction and segments orientation (Figure C1).
$\Phi(z)$	*Muskhelishvili*'s [1953] complex potential.
η_m	roots of the Chebyshev polinomial $U_{M-1}(\eta)$ (C8).
$\kappa = 3 - 4\nu$	elastic coefficient for plain strain condition.
$\lambda = 2c/d$	dimensionless segment size (Appendix C).
ν	Poisson's ratio.
θ_r	angle between the rth crack and x axis in (A7).

$\sigma(z)$	normal external load on the joint surface (Appendix A).
σ_{ij}	stress tensor.
σ_∞	remote stress perpendicular to the joints.
$\tau(z)$	tangential external load on the joint surface (Appendix A).
$\tau = \xi - \eta$	auxiliary variable in (C2) and (C3).
ξ_m	roots of the Chebyshev polinomial $T_M(\xi)$ in (C8).
$\zeta = \xi + i\eta$	dimensionless complex variable.
$\xi = x/c,\ \eta = y/c$	dimensionless rectangular coordinates.

[52] **Acknowledgments.** We thank the Associate Editor D. R. Schmitt and reviewer J. A. Hudson as well as the anonymous reviewer for their many helpful comments on an earlier version of this manuscript. The paper has considerably improved as a result of their diligent efforts. The authors are grateful to T. Bai, B. Berkowitz, B. J. Carter, A. Chudnovsky, F. Cornet, J. Desroches, E. Detournay, V. Dunayevsky, A. V. Dyskin, A. R., Ingraffea, M. J. Mayerhofer, R. P. Lowell, E. Pasternak, L. M. Ring, and M. D. Zoback for useful discussions. The authors are especially indebted to P. Dijk, D. D. Pollard, Z. Reches, and J. Shlyapobersky for many constructive suggestions as well as to J. C. Santamarina for his invaluable input that helped to design the physical experiment described in section 4. They also would like to acknowledge the courtesy of B. J. Carter and Z. Reches, who kindly sent the photographs shown in Figures 1a and 1b, respectively. The work was supported by the U.S. National Science Foundation (grants CMS-9896136, OCE-0221974, and OCE-9896021) and the U.S.-Israel Binational Science Foundation (grant 9800135).

References

Aliabadi, M. H., and D. P. Rooke (1991), *Numerical Fracture Mechanics*, 276 pp., Kluwer Acad., Norwell, Mass.

Bai, T., and D. D. Pollard (2001), Getting more for less: The unusual efficiency of fluid flow in fractures, *Geophys. Res. Lett.*, *28*, 65–68.

Bai, T., D. D. Pollard, and M. R. Gross (2000), Mechanical prediction of fracture aperture in layered rocks, *J. Geophys. Res.*, *105*, 707–721.

Becker, A., and M. R. Gross (1996), Mechanism for joint saturation in mechanically layered rocks: An example from southern Israel, *Tectonophysics*, *257*, 223–237.

Benthem, J. P., and W. T. Koiter (1973), Asymptotic approximations to crack problems, *Methods of Analysis and Solutions of Crack Problems*, edited by G. C. Sih, pp. 131–178, Wolters-Noordhoff, Groningen, Netherlands.

Berkowitz, B. (1994), Modelling flow and contaminant transport in fractured media, in *Advances in Porous Media*, vol. 2, edited by Y. Corapcioglu, pp. 395–449, Elsevier Sci., New York.

Chen, Y. Z. (1995), A survey of new integral equations in plane elasticity crack problem, *Eng. Fract. Mech.*, *51*, 97–134.

Chudnovsky, A., A. Dolgopolsky, and M. Kachanov (1987), Elastic interaction of a crack with a microcrack array-I. Formulation of the problem and general form of the solution, *Int. J. Solids Struct.*, *23*((1)1), 1–10.

Cosgrove, J. W. (1997), Fluid induced fractures in sediments and rocks and the use of desiccation fractures as mechanical analogues, *J. Geol. Soc. China*, *40*, 243–260.

Datsyshin, A. P., and M. P. Savruk (1974), Integral equations of the plane problem of crack theory, *J. Appl. Math. Mech.*, *38*, 677–686.

David, C. (1993), Geometry of flow paths for fluid transport in rocks, *J. Geophys. Res.*, *98*, 12,267–12,278.

Delameter, W. R., G. Herrmann, and D. M. Barnett (1975), Weakening of an elastic solid by a rectangular array of cracks, *Trans. ASME J. Appl. Mech.*, *42*, 74–80.

Delaney, P. T., and D. D. Pollard (1981), Deformation of host rocks and flow of magma during growth of minette dikes and breccia-bearing intrusions near Ship Rock, New Mexico, *U.S. Geol. Surv. Prof.*, *1202*.

Delaney, P. T., D. D. Pollard, J. I. Ziony, and E. H. McKee (1986), Field relation between dikes and joints: Emplacement processes and paleostress analysis, *J. Geophys. Res.*, *91*, 4920–4938.

Demidovich, B. P., and I. A. Maron (1987), *Computational Mathematics*, 688 pp., Mir, Moscow.

Dershowitz, W. S., and H. H. Einstein (1988), Characterizing joint geometry with joint system models, *Rock Mech. Rock Eng.*, *21*, 21–51.

Du, Y., and A. Aydin (1991), Interaction of multiple cracks and formation of echelon crack arrays, *Int. J. Numer. Anal. Methods Geomech.*, *15*, 205–218.

Dyskin, A. V., and H.-B. Mühlhaus (1995), Equilibrium bifurcations in dipole asymptotic model of periodic crack arrays, in *Continuum Models for Materials With Micro-Structure*, edited by H. B. Mühlhaus, pp. 69–104, John Wiley, New York.

Engelder, T., and A. Lacazette (1990), Natural hydraulic fracturing, in *Rock Joints: Proceedings of the International Symposium on Rock Joints, Loen, Norway, June 4–6, 1990*, edited by N. Barton and O. Stephansson pp. 35–43, A. A. Balkema, Brookfield, Vt.

Engelder, T., P. Hagin, B. Haith, A. Lacazette, S. Loewy, D. McConaughy, and A. Younes (1999), The Catskill Delta Complex: Analog for modern continental shelf and delta sequences containing overpressured sections, Seal Evaluation Consortium (SEC) Field Trip, Pa. State Univ., University Park.

Erdogan, F., and G. D. Gupta (1972), On the numerical solution of singular integral equations, *Q. Appl. Math.*, *29*, 525–534.

Erdogan, F., G. D. Gupta, and T. S. Cook (1973), Numerical solution of singular integral equations. *Methods of Analysis and Solutions of Crack Problems*, edited by G. C. Sih, pp. 368–425, Wolters-Noordhoff, Groningen, Netherlands.

Fischer, M. P., M. R. Gross, T. Engelder, and R. J. Greenfield (1995), Finite-element analysis of the stress distribution around a pressurized crack in a layered elastic medium: Implications for the spacing of fluid-driven joints in bedded sedimentary rock, *Tectonophysics*, *247*, 49–64.

Galybin, A. N. (1998), Stress intensity factors for two periodical rows of collinear cracks, *Eng. Fract. Mech.*, *59*, 281–288.

Gangi, A. F. (1978), Variation of whole and fractured porous rock permeability with confining pressure, *Int. J. Rock Mech. Min. Sci. Geomech. Abstr.*, *15*, 249–257.

Gavrilenko, P., and Y. Gueguen (1989), Pressure dependence of permeability: A model for cracked rocks, *Geophys. J. Int.*, *98*, 159–172.

Germanovich, L. N., and D. K. Astakhov (2004), Stress-dependent permeability and fluid flow through parallel joints, *J. Geophys. Res.*, *108*, doi:10.1029/2002JB002133, in press.

Germanovich, L. N., D. K. Astakhov, M. J. Mayerhofer, J. Shlyapobersky, and L. M. Ring (1997a), Hydraulic fracture with multiple segments, part I: Observations and model formulation, *Int. J. Rock Mech. Min. Sci. Geomech. Abstr.*, *34*, 471.

Germanovich, L. N., L. M. Ring, D. K. Astakhov, J. Shlyapobersky, and M. J. Mayerhofer (1997b), Hydraulic fracture with multiple segments, part II: Effect of interaction, *Int. J. Rock Mech. Min. Sci. Geomech. Abstr.*, *34*, 472.

Germanovich, L. N., D. K. Astakhov, J. Shlyapobersky, M. J. Mayerhofer, C. Dupont, and L. M. Ring (1998a), Modeling Multisegmented hydraulic fracture in two extreme cases: No leakoff and dominating leakoff, *Int. J. Rock. Mech. Min. Sci. Geomech. Abstr.*, *35*, 551–554.

Germanovich, L. N., D. K. Astakhov, J. Shlyapobersky, and L. M. Ring (1998b), A Model of Hydraulic Fracture with Parallel Segments, in *Modeling and Simulation Based Engineering*, edited by S. N. Atluri and P. E. O'Donoghue, pp. 1261–1268, Tech Sci., Encino, Calif.

Germanovich, L. N., R. P. Lowell, and D. K. Astakhov (2000), Stress dependent permeability and the formation of seafloor event plumes, *J. Geophys. Res.*, *105*, 8341–8354.

Gladwell, G. M. L., and A. H. England (1977), Orthogonal polynomial solutions to some mixed boundary-value problems in elasticity theory, *Q. J. Mech. Appl. Math.*, *30*(2), 175–185.

Gross, R. M. (1993), The origin and spacing of cross joints: Examples from the Monterey Formation, Santa Barbara coastline, California, *J. Struct. Geol.*, *15*, 737–751.

Hayden, H. W., W. G. Moffatt, and J. Wulff (1965), *The Structure and Properties of Materials*, 247 pp., John Wiley, New York.

Helgeson, D. E., and A. Aydin (1991), Characteristics of joint propagation across layer interfaces in sedimentary rocks, *J. Struct. Geol.*, *13*, 897–911.

Hobbs, D. W. (1967), The formation of tension joints in sedimentary rocks: An explanation, *Geol. Mag.*, *104*, 550–556.

Hu, K. X., A. Chandra, and Y. Huang (1993), Multiple void-crack interaction, *Int. J. Solids Struct.*, *30*, 1473–1489.

Hudson, J. A., and S. D. Priest (1979), Discontinuity rock mass geometry, *Int. J. Rock Mech. Min. Sci. Geomech. Abstr.*, *16*, 339–362.

Isida, M. (1970), Analysis of stress intensity factors for plates containing random array of cracks, *Bull. JSME*, *13*(59), 635–642.

Isida, M. (1971), Effect of width and length on stress intensity factors of internally cracked plates under various boundary conditions, *Int. J. Fract. Mech.*, *7*, 301–316.

Isida, M. (1973), Method of Laurent series expansion for internal crack problems, in *Methods of Analysis and Solutions of Crack Problems*, edited by G. C. Sih, pp. 56–130, Wolters-Noordhoff, Groningen, Netherlands.

Jeffrey, R. G., L. Vandamme, and J.-C. Roegiers (1987), Mechanical interactions in branched or subparallel hydraulic fractures, paper SPE 16422

presented at the SPE/DOE Low Permeability Reservoirs Symposium, Soc. of Pet. Eng., Denver, Colo., 18–19 May.
Ji, S., and K. Saruwatari (1998), A revised model for the relationship between joint spacing and layer thickness, *J. Struct. Geol.*, *20*, 1495–1508.
Kachanov, M. (1987), Elastic solids with many cracks: A simple method of analysis, *Int. J. Solids Struct.*, *23*(1), 23–43.
Kachanov, M. (1993), Elastic solids with many cracks and related problems, *Adv. Appl. Mech.*, *30*, 259–445.
Kishida, M., and M. Asano (1984), A study of interference of three parallel cracks, *Eng. Fract. Mech.*, *19*, 531–538.
Koiter, W. T. (1961), An infinite row of parallel cracks in an infinite elastic sheet, in *Problems of Continuum Mechanics*, 246–259, Soc. for Ind. And Appl. Math., Philadelphia, Pa.
Korn, G. A., and T. M. Korn (2000), *Mathematical Handbook for Scientists and Eng.*, Dover, Mineola, N. Y.
Lachenbruch, A. H. (1961), Depth and spacing of tension cracks, *J. Geophys. Res.*, *66*, 4273–4292.
Ladeira, F. L., and N. J. Price (1981), Relationship between fracture spacing and bed thickness, *J. Struct. Geol.*, *3*, 179–183.
Lam, K. Y., and S. P. Phua (1991), Multiple crack interaction and its effect on stress intensity factor, *Eng. Fract. Mech.*, *40*, 585–592.
Landau, L. D., and E. M. Lifshitz (1986), *Theory of Elasticity*, 3rd English ed., 187 pp., Pergamon, New York.
Liu, G. T., and R. Z. Zhou (1990), The strength of a finite body with multiple cracks, *Eng. Fract. Mech.*, *35*, 67–78.
Long, J. C. S., et al. (1996), *Rock Fractures and Fluid Flow, Contemporary Understanding and Applications*, 551 pp., Natl. Acad. Press, Washington, D. C.
Martel, S. J., and W. A. Boger (1998), Geometry and mechanics of secondary fracturing around small three-dimensional faults in granitic rock, *J. Geophys. Res.*, *103*, 21,299–21,314.
McCartney, L. N., and T. A. E. Gorley (1987), Variable method of calculating stress intensity factors for cracks in plates, in *Numerical Methods in Fracture Mechanics*: *Proceedings of the 4th International Conference, San Antonio, Tex., 23–27 March 1987*, edited by A. R. Luxmoore et al., pp. 55–72, Pineridge, Swansea, U.K.
McMaster-Carr Supply Company (2003), Catalog No 109, Atlanta, Ga.
McQuillan, H. (1973), Small-scale fracture density in Asmari formation of southwest Iran and its relation to bed thickness and structural setting, *Am. Assoc. Petrol. Geol. Bull.*, *57*, 2367–2385.
Murakami, Y., (Ed.) (1987), *Stress Intensity Factor Handbook*, Pergamon, New York.
Muskhelishvili, N. I. (1953), *Some Basic Problems of the Mathematical Theory of Easticity*, Wolters-Noordhoff, Groningen, Netherlands.
Muskhelishvili, N. I. (1992), *Singular Integral Equations*, Dover, Mineola, N. Y.
Narr, W., and J. Suppe (1991), Joint spacing in sedimentary rocks, *J. Struct. Geol.*, *13*, 1037–1048.
Nehlig, P., and T. Juteau (1988), Flow porosities, permeabilities and preliminary data on fluid inclusions and fossil geothermal gradients in the crustal sequence of the Sumail ophiolite (Oman), *Tectonophysics*, *151*, 199–221.
Nolte, K. G. (1987), Discussion of influence of geologic discontinuities on hydraulic fracture propagation, *JPT J. Pet. Technol.*, *39*, 998.
Olson, J. E. (1993), Joint pattern development: Effects of subcritical crack growth and mechanical crack interaction, *J. Geophys. Res.*, *98*, 12,251–12,265.
Olson, J. E., and D. D. Pollard (1991), The initiation and growth of en echelon veins, *J. Struct. Geol.*, *13*, 595–608.
Palmer, I. D., and R. W. Veatch Jr. (1990), Abnormally high fracturing pressures in step-rate tests, *SPE Prod. Eng., paper 16902*, 315–323.
Panasyuk, V. V., M. P. Savruk, and A. P. Datsyshyn (1977), A general method of solution of two-dimensional problems in the theory of cracks, *Eng. Fract. Mech.*, *9*, 481–497.
Parker, A. P. (1981), *The Mechanics of Fracture and Fatigue*, 167 pp., E. & F. N. Spon, New York.
Pollard, D. D., and A. Aydin (1988), Progress in understanding jointing over the past century, *Geol. Soc. Am. Bull.*, *100*, 1181–1204.
Pollard, D. D., and P. Segall (1987), Theoretical displacements and stresses near fractures in rocks: With applications to faults, joints, veins, dikes and solution surfaces, in *Fracture Mechanics of Rock*, edited by B. K. Atkinson, pp. 277–349, Academic, San Diego, Calif.
Renshaw, C. E., and J. C. Park (1997), Effect of mechanical interactions on the scaling of fracture length and aperture, *Nature*, *386*, 482–484.
Reches, Z. (1998), Tensile fracturing of stiff rock layers under triaxial compressive stress states, *Int. J. Rock Mech. Min. Sci.*, *35*, 4–5.
Reches, Z., and D. A. Lockner (1994), Nucleation and growth of faults in brittle rocks, *J. Geophys. Res.*, *99*, 18,159–18,173.
Rooke, D. P., and D. J. Cartwright (1976), *The Compendium of Stress Intensity Factors*, 330 pp., Her M. Stationary Off., London.
Sagy, A., Z. Reches, and I. Roman (2001), Dynamic fracturing: Field and experimental observations, *J. Struct. Geol.*, *23*, 1223–1239.
Savruk, M. P. (1981), *Two-Dimensional Elastic Problems for Bodies With Cracks* (in Russian), Naukova Dumka, Kiev.
Secor, D. T. (1965), Role of fluid pressure in jointing, *Am. J. Sci.*, *263*, 633–646.
Sih, G. C. (1973), *Handbook of Stress Intensity Factors*, vol. 1, 420 pp., Lehigh Univ. Press, Bethlehem, Pa.
Smith, E. (1966), The opening of parallel cracks by an applied tensile stress, *Int. J. Eng. Sci.*, *4*(1), 41–52.
Sneddon, I. N. (1951), *Fourier Transforms*, 542 pp., McGraw-Hill, New York.
Tada, H., P. C. Paris, and G. R. Irwin (1985), *The Stress Analysis of Cracks Handbook*, Paris Prod., St. Louis, Mo.
Theocaris, P. S., and A. C. Chrysakis (1983), Stress intensity factors at a finite number of parallel, equal cracks: A mixed-mode problem, *Solid Mech. Arch.*, *8*(4), 313–335.
Tsang, Y. W., and P. A. Witherspoon (1981), Hydromechanical behavior of a deformable rock fracture subject to normal stress, *J. Geophys. Res.*, *86*, 9287–9298.
van Everdingen, D. A. (1995), Fracture characteristics of the sheeted dike complex, Troodos ophiolite, Cyprus: Implications for permeability of oceanic crust, *J. Geophys. Res.*, *100*, 19,957–19,972.
Wawrzynek, P. A., and A. R. Ingraffea (1991), Discrete modelling of crack propagation: Theoretical aspects and implementation issues in two and three dimensions, *Rep. 91-5*, Sch. of Civ. and Environ. Eng., Cornell Univ., Ithaca, N. Y.
Willemse, E. J. M., D. D. Pollard, and A. Aydin (1996), Three-dimensional analyses of slip distributions on normal fault arrays with consequences for fault scaling, *J. Struct. Geol.*, *18*, 295–309.
Zhao, G., and A. M. Johnson (1992), Sequence of deformations recorded in joints and faults, Arches National Park, Utah, *J. Struct. Geol.*, *14*, 225–236.

L. N. Germanovich, School of Civil and Environmental Engineering, Georgia Institute of Technology, Atlanta, GA 30332-0355, USA. (leonid@ce.gatech.edu)

D. K. Astakhov, Pinnacle Technologies, Inc., 5301 Office Park Drive, Suite 370, Bakersfield, CA 93309-0654, USA. (dmitriy.astakhov@pinntech.com)